2014

Broad Bandwidth, All-fiber, Thulium-doped Photonic Crystal Fiber Amplifier for Potential Use in Scaling Ultrashort Pulse Peak Powers

Alex Sincore
University of Central Florida

BROAD BANDWIDTH, ALL-FIBER, THULIUM-DOPED PHOTONIC CRYSTAL FIBER AMPLIFIER FOR POTENTIAL USE IN SCALING ULTRASHORT PULSE PEAK POWERS

by

ALEX SINCORE
B.S. University of Florida, 2012

A thesis submitted in partial fulfillment of the requirements
for the degree of Master of Science
in the College of Optics and Photonics
at the University of Central Florida
Orlando, Florida

Spring Term
2014

Major Professor: Martin Richardson

ABSTRACT

Fiber based ultrashort pulse laser sources are desirable for many applications; however generating high peak powers in fiber lasers is primarily limited by the onset of nonlinear effects such as self-phase modulation, stimulated Raman scattering, and self-focusing. Increasing the fiber core diameter mitigates the onset of these nonlinear effects, but also allows unwanted higher-order transverse spatial modes to propagate. Both large core diameters and single-mode propagation can be simultaneously attained using photonic crystal fibers.

Thulium-doped fiber lasers are attractive for high peak power ultrashort pulse systems. They offer a broad gain bandwidth, capable of amplifying sub-100 femtosecond pulses. The longer center wavelength at 2 μm theoretically enables higher peak powers relative to 1 μm systems since nonlinear effects inversely scale with wavelength. Also, the 2 μm emission is desirable to support applications reaching further into the mid-IR.

This work evaluates the performance of a novel all-fiber pump combiner that incorporates a thulium-doped photonic crystal fiber. This fully integrated amplifier is characterized and possesses a large gain bandwidth, essentially single-mode propagation, and high degree of polarization. This innovative all-fiber, thulium-doped photonic crystal fiber amplifier has great potential for enabling high peak powers in 2 μm fiber systems; however the current optical-to-optical efficiency is low relative to similar free-space amplifiers. Further development and device optimization will lead to higher efficiencies and improved performance.

TABLE OF CONTENTS

LIST OF FIGURES

LIST OF TABLES

LIST OF ABBREVIATIONS

ASE	Amplified spontaneous emission
CBG	Chirped Bragg grating
CPA	Chirped pulse amplification
CW	Continuous-wave lasing
DC	Double-clad fiber
FBG	Fiber Bragg gratings
HOM	Higher-order modes
LMA	Large mode area
LCF	Leaky channel fibers
LP	Linearly polarized modes
LPF	Large-pitch photonic crystal fibers
MA	Mode-field adaptors
MFA	Mode field area
ML	Mode-locked
MMI	Multimode interference
MOPA	Master oscillator, power amplifier
NA	Numerical aperture
NLE	Nonlinear effects
PCF	Photonic crystal fiber
PER	Polarization extinction ratio
PM	Polarization maintaining fiber
SIF	Step-index fiber

SBS	Stimulated Brillouin scattering
SPM	Self-phase modulation
SRS	Stimulated Raman scattering
SSFS	Soliton self-frequency shift
TFB	Tapered fiber bundles
Tm	Thulium (specifically the laser-active ion Tm^{3+})
USP	Ultrashort pulse

CHAPTER 1: INTRODUCTION

Lasers operating in the ultrashort pulse (USP) regime, with pulse durations from picoseconds to femtoseconds, are useful for applications such as materials processing, remote sensing, laser spectroscopy, terahertz generation, high-intensity physics, medicine, and many others [1-7]. For several of these uses, it is advantageous to produce high peak power/high energy in addition to ultrashort pulse duration. Consequently, methods are continuously being investigated to scale peak powers in USP systems.

Most high peak power USP systems use bulk solid-state media, producing record output powers at the expense of large spatial footprints and numerous free-space optics. Whereas free-space systems are sensitive to misalignment; fully integrated fiber lasers offer compact, environmentally stable, and modular systems. Because of these key advantages, there has been growing interest in scaling peak powers specifically in fiber-based USP systems.

This thesis focuses on developments and future perspectives in scaling peak powers in USP fiber systems, with primary interest in evolving towards an "all-fiber" structure. "All-fiber" placed in quotes will signify the use of fiberized components, which may include free-space optics packaged to virtually eliminate alignment sensitivity. To further advance peak power scaling in a custom-built, 3 MW, sub-500 femtosecond 2 μm system [8], a novel all-fiber pump combiner that incorporates a thulium-doped photonic crystal fiber amplifier is characterized. This component is suitable to mitigate multimode interference, which degraded the compressed pulse quality of the 3 MW system [8].

In Chapter 2, optical propagation in fibers is briefly discussed followed by the advancements in fiber laser geometries. Many of the unwanted nonlinear effects, as well as fiber facet damage, scale with mode field area. Therefore, an important area of research has been to enlarge fiber diameters while maintaining single transverse mode propagation. In section 2.3, a microstructured fiber, known as photonic crystal fiber, is presented. This design has successfully enabled production of ultra large mode area fibers with single-mode beam quality. Lastly, because the experimental work described in this thesis has been performed at 2 μm using thulium-doped fibers, a brief description of thulium's properties and benefits are provided in section 2.4.

In Chapter 3, limitations and recent progress in scaling USP fiber systems are discussed. Wave propagation in fibers is typically associated with relatively long distances and tight confinement, making nonlinear phenomena key limitations. The nonlinear limitations that will be considered in section 3.1 are: self-focusing, self-phase modulation, stimulated Raman scattering, and stimulated Brillouin scattering. Lastly, pulse degradation due to multimode interference is detailed in section 3.2. This was the limiting factor discovered in the 3 MW USP system, and the component investigated in Chapter 5 is suggested to overcome multimode interference.

In Chapter 4, complications and realizations of an "all-fiber" high power system is examined. Section 4.1 lists a brief overview of the fiberized components required and their progress, with special emphasis on components developed for 2 μm. Due to the nature of this report, section 4.1.1 specifically discusses step-index fiber pump combiners. Lastly, section 4.2 displays some recent work toward "all-fiber" USP systems.

In Chapter 5, an all-fiber pump combiner that includes the aforementioned photonic crystal fiber is characterized for potential use as an amplifier in the custom-built, 3 MW USP system. While the slope efficiency is low at 22.1 %, the beam quality is excellent with $M^2 < 1.1$. Also, no spectral modulations are observed when amplifying a broadband spontaneous emission source. The lack of spectral modulations corroborates the quasi-single-mode beam quality, demonstrating the potential of this component to avoid multimode interference during amplification. This chapter will discuss possible optimization in the pump combiner design to improve slope efficiencies as well as eliminate random polarization state fluctuations that were observed.

Lastly, Chapter 6 concludes this thesis with an overview of peak power scaling and future research efforts in USP thulium-fiber system in LPL. Possible implementations and necessary changes are provided to enlighten the multiple paths this research could take.

CHAPTER 2: FIBER STRUCTURE FOR USE IN LASERS

Optical fibers are circularly symmetric waveguides, commonly produced using silica glass. To facilitate light guidance by total internal reflection, the properties of the fiber are modified where the core region has a higher index of refraction than the cladding region. The design incorporating a discrete index change is known as a step-index fiber (SIF) [9-11]. Figure 1a is an example of a light ray entering a SIF at an entrance angle, θ_0, then confined to the core by a critical angle, θ_c. Figure 1b represents the index of refraction, n, for radial positions along the SIF, where n_0 is the refractive index of the outside environment. The fiber core and cladding radius are denoted by a and b, respectively.

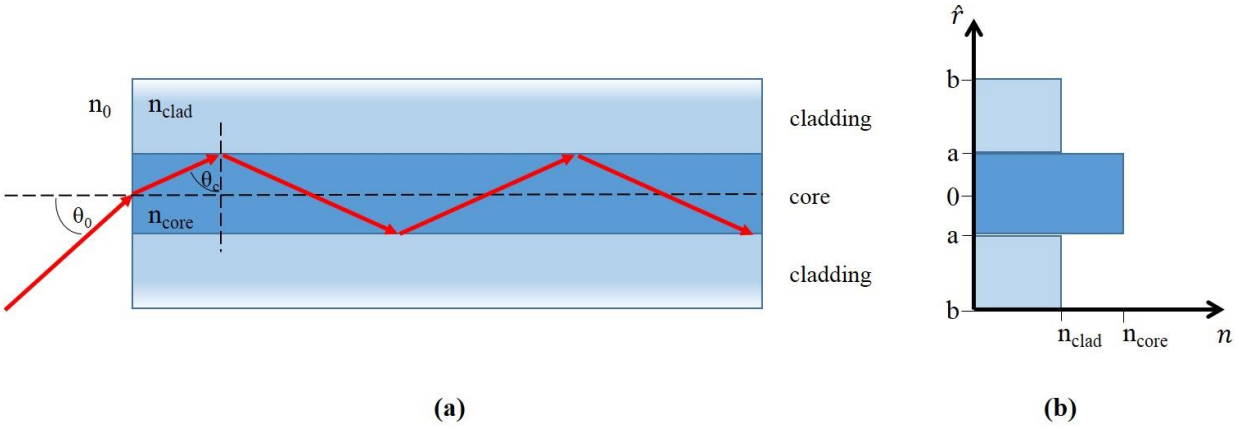

Figure 1. (a) Ray diagram for a fiber waveguide. (b) Refractive index profile for a SIF.

Using the electromagnetic wave equations and imposing the fiber boundary conditions, many interesting consequences and useful formalisms appear. The important ones for this discussion are waveguide modes, mode field area (MFA), V-number, and numerical aperture (NA), which are outlined in section 2.1. Section 2.2 will present the developments of polarization maintaining (PM)

fibers, double-clad (DC) fibers, MFA expansions in SIF, and their successful impacts on fiber lasers. Section 2.3 introduces the novel fiber design – photonic crystal fibers (PCF). These fibers provided one avenue for further MFA scaling with innovative microstructured architectures. Lastly, section 2.4 overviews the rare-earth ion thulium (Tm^{3+}) when doped in silica fibers, and the benefits of thulium's 2 μm emission wavelength.

2.1 Waveguide Modes and Useful Relations

After solving the wave equation confined to radial symmetry (a fiber) and assuming linear polarization (a preferred feature), the possible transverse modes that can propagate are denoted as LP_{lm} (LP stands for linear polarization) [11]. The fundamental mode, LP_{01}, is a Bessel function but can be approximated as a Gaussian distribution [12], and is the preferred mode for many laser systems. It has the simplest propagation characteristics and can be focused to the smallest spot. Concerning the majority of high peak power USP lasers, all other modes are undesirable and are known as higher-order modes (HOM). Figure 2 illustrates the spatial profile for some of these modes.

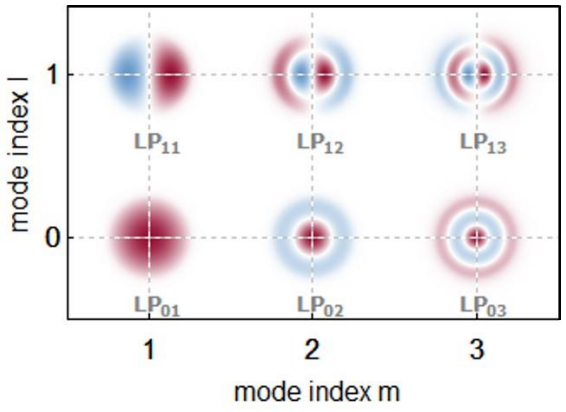

Figure 2. Electric field profile for LP_{lm} modes, red and blue denote opposite phase [13].

As will be seen in Chapter 3, many nonlinear effects scale with MFA and not necessarily core diameter. MFA is the effective spatial area of the electromagnetic wave, and is generally defined by Equation 1, where $I(r)$ is the radial intensity profile [14].

$$\mathrm{MFA} = \frac{2\pi\left(\int_0^\infty I(r) r dr\right)^2}{\left(\int_0^\infty I^2(r) r dr\right)} \quad (1)$$

For Gaussian beams, the MFA corresponds to the area using the $1/e^2$ beam radius (where intensity drops to $1/e^2$ of maximum), or simply: $\mathrm{MFA_{Gaussian}} \cong \pi w_0^2$ [14, 15]. For SIF and Gaussian beam propagation, scaling core diameter consequently scales MFA.

The V-number is a useful parameter for determining if SIF is single-mode. Single-mode behavior for SIF is ensured for V < 2.405 because HOM cannot be supported [11, 12]. NA is another useful quantity, it defines the maximum entrance angle (θ_0 from Figure 1) that still allows coupling into the core. These two parameters are expressed in Equations 2 and 3.

$$\mathrm{NA} = n_0 \cdot \sin(\theta_0) = \sqrt{n_{core}^2 - n_{cladding}^2} \quad (2)$$

$$V = \frac{2\pi}{\lambda} \cdot a \cdot \mathrm{NA} \quad (3)$$

As seen in Equation 3, for a given wavelength λ, the only way to scale core diameter and maintain single-mode operation is to decrease NA. Current fiber fabrication limits NA ≥ 0.05 for SIF, allowing theoretical single-mode core diameters of 30 μm for 2 μm light, and 15 μm for 1 μm light. Therefore, MFA are limited to ~200 μm^2 for 1 μm light. Because of this limit, extensive research

is continually being conducted on ways to scale MFA in SIF while remaining single-mode. The next section discusses these techniques, as well as the successes of PM and DC fibers.

2.2 Advancements in Step-Index Fiber Laser Design

2.2.1 Polarization Maintaining Fibers

For an ordinary SIF as pictured in Figure 1, coiling and mechanical stress can induce small birefringence fluctuations in the fiber. Therefore, a linear input polarization will react to this random birefringence to produce a noisy output polarization. Stable, highly polarized outputs are useful for many applications [16]. So to combat this, PM fibers were developed that incorporate thermal-expansion-contrasting stress rods (usually boron doped), such as the commercial PANDA geometry seen in Figure 3 [17]. These rods generate strong stress-induced birefringence along the fiber. By launching linearly polarized light either parallel or perpendicular to these stress rods, the output polarization will remain linear as well. The polarization contrast can be quantified by the polarization extinction ratio (PER) defined in Equation 4.

$$\text{PER} = 10 \cdot \log\left(\frac{\text{Power in preferred polarization}}{\text{Power not in preferred polarization}}\right) \quad (4)$$

PER greater than 15 dB is routinely demonstrated in PM fiber lasers, even for high power systems [18, 19]. Advanced designs, such as elliptical cores and air-filled stress rods, can lead to single polarization fibers with PER ~ 60 dB [20].

2.2.2 Double-Clad Fibers

For fiber lasers, the core is doped with an active ion for a gain medium. To initate lasing, a pump source must be applied to excite the ions. High power pump sources for fiber laser applications are usually diode based, typically emitting multimode and high NA light. As discussed in section 2.1, the core is preferentially designed to maintain single-mode beam quality, which prevents the coupling of multimode pump diodes into the core. To circumvent these challenges, DC fibers were developed that employ a higher-index inner cladding surrounded by a lower-index outer cladding, seen in Figure 3 [21]. Therefore, high power multimode pump sources can be coupled into a large area inner cladding that overlaps the core gain medium. This permits longer pump absorption lengths, and by 1999 enabled output powers exceeding 100 W from a continous-wave (CW) fiber laser [22, 23].

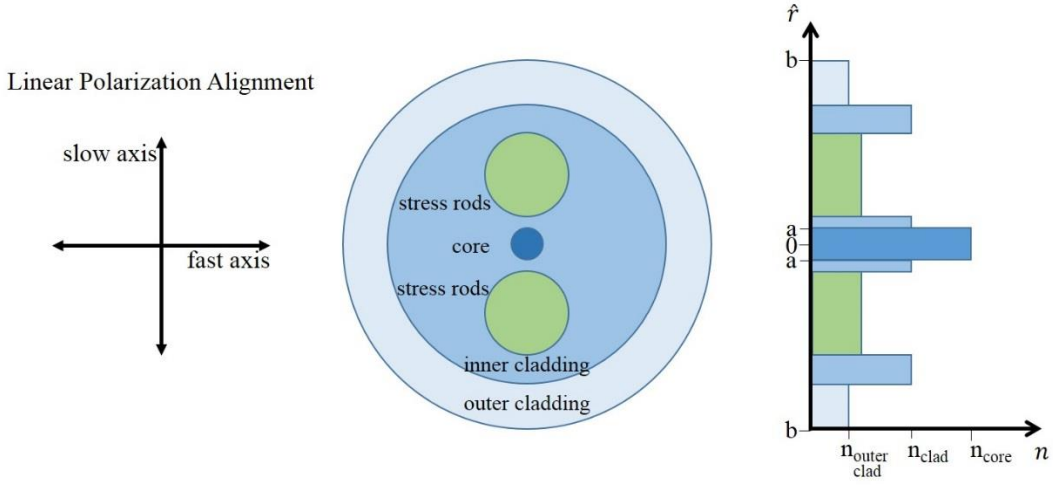

Figure 3. PM-DC-SIF. Left: Preferred input polarization to maintain linear output polarization. Right: Cross-sectional refractive index profile.

2.2.3 Techniques to Increase MFA in SIF

With the addition of PM-DC fibers, fiber lasers could be constructed with a high degree of polarization, and large output powers due to increased pump coupling. While the DC design enabled average power scaling, methods to increase MFA while remaining single-mode were necessary to mitigate nonlinear effects and damage, such as for peak power scaling.

A simple method commonly used to improve the mode quality of large mode area (LMA) SIF is bending the fiber to induce HOM loss. Coiling the fiber causes confined radiation to leak out [24, 25], and has been shown to occur more strongly for HOM than the fundamental mode [26, 27]. By taking advantage of this principle, LMA SIF that allow few HOM, with $V > 2.405$, can be coiled to preferentially cause enough HOM loss to overcome their gain. This then produces an effectively single-mode output. For example, the LMA Tm:SIF amplifier used in the 3 MW system was shown to provide reduced HOM content with 10 cm coiling diameters [28]. However, tight bending causes mode-field distortion, reduced MFA, and loss for the fundamental mode. With all taken into consideration, effective single-mode MFA are limited to $< 400\ \mu m^2$ at 1 μm wavelengths and 0.06 NA by using simple HOM bend loss techniques [29], a factor of ~2 increase from conventional SIF.

While HOM bend suppression is the most common method, many other SIF designs have been proposed and demonstrated for single-mode MFA scaling. Some of these techniques include: gain guided, index anti-guided fibers [30, 31]; helical core fibers [32]; gain filtering fibers [33]; chirally-coupled core fibers [34]; or by using a long-period grating to couple HOM to fundamental

mode [35]. Optimal seed coupling, with fiber bending and specialized techniques, have seen effectively single-mode excitation of SIF with MFA up to ~700 μm^2 [36].

2.3 Photonic Crystal Fibers

Even though impressive MFAs have been demonstrated in SIF via the aforementioned techniques, a different notable approach is photonic crystal fiber (PCF) [37, 38]. PCF abandon the conventional SIF refractive index pedestal seen in Figure 1, and employ periodic structure in the fiber. These microstructured fibers have opened a breadth of research, too plentiful to be considered here [39-42]. Relevant to this report, PCF with solid cores are discussed.

PCF structure incorporates an array of periodically spaced holes (typically filled with air, as in this research) surrounding a solid-core region, seen in Figure 4. The guiding properties are then dictated by the diameter d, and pitch Λ, of the holes [43]. When these structure sizes are on the order of the wavelength, the medium can be described with an effective refractive index, which is less than the solid core [44]. This effectively operates as a SIF. This effective-medium also permits a V-number parameter [45, 46], and has been shown that tuning d and Λ can allow endlessly single-mode operation [47].

Consequently, by optimizing d and Λ, PCF offers much greater flexibility in manufacturing the "index-step" than SIF. This is attractive for fiber amplifiers because it permits fabrication of low NA, and very large MFA while simultaneously enabling effective single-mode operation. Both ytterbium and thulium-doped PCF utilizing this design have enabled MFA ~ 1000 μm^2 with $M^2 <$ 1.2 [48, 49] ($M^2 \sim 1$ is considered essentially single mode, see section 5.3.2). This is a factor of ~5 increase from conventional SIF. Also, by surrounding the central region with a larger air-filled

cladding, a large NA DC-PCF is produced, seen in Figure 4. Stress rods can also be introduced in the same fashion as SIF to facilitate highly polarized outputs.

Increasing the MFA over 1000 μm^2 in PCF hinders the fiber rigid, and unable to be bent due to fracture or large bend losses. While this ruins one benefit of fiber systems, these rod-like-PCFs enable ultra large MFA that were previously inaccessible. Ytterbium-doped rod-PCFs have been reported with MFA of 4000 μm^2 [50], and upwards of ~5500 μm^2 with $M^2 = 1.3$ [51]. Recently, a thulium-doped rod-PCF with MFA > 2800 μm^2 and $M^2 < 1.3$ was demonstrated [52].

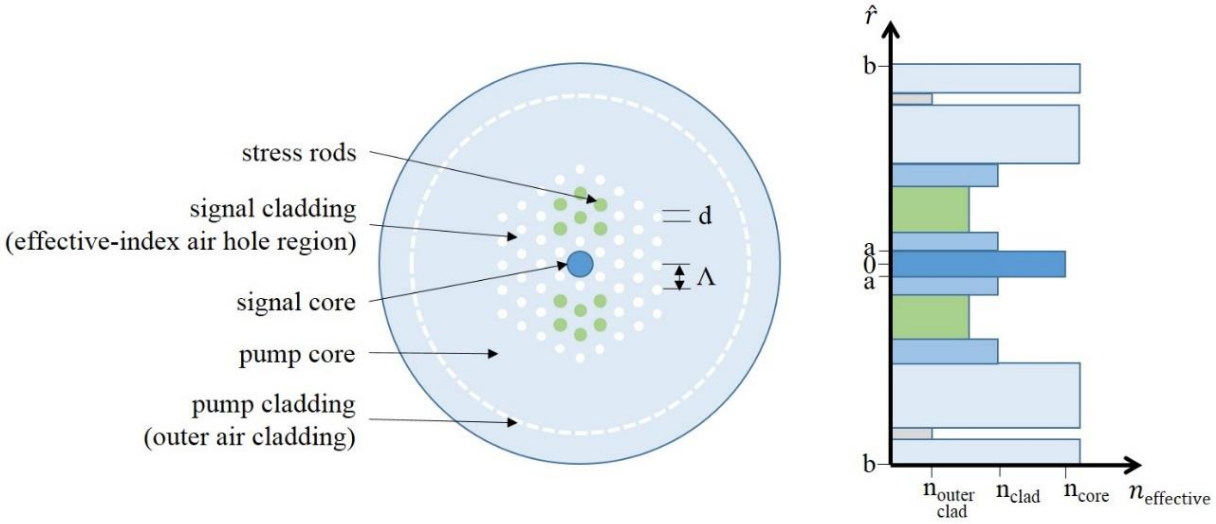

Figure 4. PM-DC-PCF cross-sectional schematic and effective-index profile: Λ – pitch, d – diameter.

While effective-index guiding PCF surpassed the effective single-mode MFA limit of SIF, it has been shown that these PCF are not strictly single-mode [53]. Proper signal launch conditions enable these systems to be operated effectively single-mode, but at high powers these HOM may cause problems. Secondly, HOM in effective-index guiding PCF overlap the core, therefore

scaling core diameters reduces the HOM discrimination relative to the fundamental mode, presenting a limit for MFA scaling. The most recent design to enable further MFA scaling with effective single-mode operation are large-pitch photonic crystal fibers (LPF), in which Λ is 10 times greater than the wavelength [54]. These designs have inherently lossy modes, and were first termed leakage channel fibers (LCF) with ytterbium-doped MFA of 3100 μm^2 [55]. Recent LPF designs de-localize HOM from overlapping the doped-core [43]. Thus, the HOM experiences little-to-no gain compared to the fundamental Gaussian-like mode, resulting in large modal discrimination. This design has demonstrated record-breaking ytterbium-doped MFA of 8600 μm^2 [56], and record-breaking thulium-doped MFA of 3100 μm^2 [57].

While record MFA have been demonstrated with PCF, some drawbacks to these designs are: high costs, short fiber lengths (~1 meter), substantial bend losses for rod-PCF, and difficulty for all-fiber integration. Large transmission losses accrue when attempting to splice to all-solid fibers, as well as the difficulty in preventing air hole collapse from the splice process. Thus, these systems primarily use free-space coupling. Nonetheless, PCF-based amplifiers have produced record peak powers/pulse energies in many fiber systems [50, 51, 56, 58-60], as detailed in section 3.3.

2.4 Thulium as a Laser Dopant

Most fiber lasers incorporate ytterbium or erbium as the active ion. These are preferentially selected for high optical-to-optical efficiencies and for their mature fiberized components in these wavelength ranges [23]. In this work, thulium is used for three main reasons: large gain bandwidth, increase in nonlinear thresholds, and applications at 2 μm. Thulium's drawbacks are namely low

efficiency, and immature fiber components for 2 μm. In this section, thulium's spectroscopic properties are presented followed by applications at 2 μm.

2.4.1 Spectroscopic Properties

Thulium is a rare-earth ion, and has a complex energy level diagram when doped in silica. The most notable feature is the wide emission range of 1.7 – 2.1 μm [61-63]. This large bandwidth is unique for rare-earth ions, and supports generation and subsequent amplification of sub-100 femtosecond transform-limited pulses. Figure 5 shows the energy level diagram for thulium, including two important effects: cross-relaxation and up-conversion.

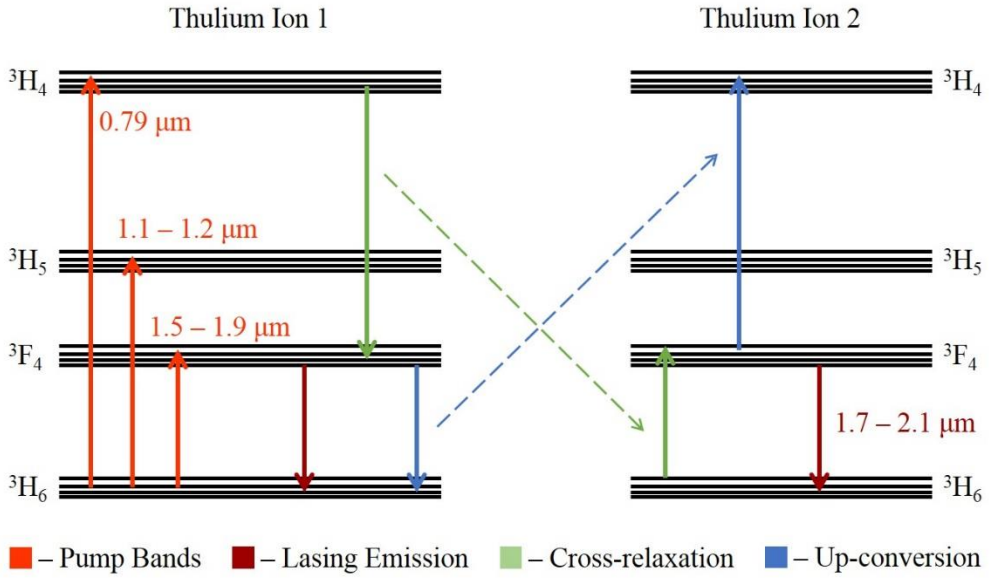

Figure 5. Energy level diagram for thulium-doped silica fiber, and energy processes that can occur between two ions.

An important aspect in choosing a pump wavelength is the quantum defect; this is approximately the loss in energy from converting one pump photon to one signal photon. The excess energy will

be transferred to heat, which must be extracted. Ideally, in-band pumping at the 1.5 – 1.9 μm regime would minimize the quantum defect. This can be accomplished using high power erbium-doped fiber lasers [64, 65]. However, these are more expensive relative to commercial pump diodes and provide less pump power. Therefore, the 0.79 μm band is used because there exist multitudes of commercially available high power pump diodes [66]. This would seem to limit optical-to-optical efficiencies to ~40 %, however cross-relaxation can theoretically increase this to ~80 % [67].

Cross-relaxation allows energy from one ion's $^3H_4 \rightarrow {}^3F_4$ transfer to excite a nearby ion from $^3H_6$ to $^3F_4$. Optimizing thulium doping concentrations, with aluminum co-doping to reduce clustering [68], have demonstrated efficiencies reaching 74 % [67]. Nonetheless, typical high power thulium-doped systems operate at 50 – 60 % efficiency, requiring forced air-cooling or water-cooled mandrels for optimal heat extraction. Furthermore, exploitation of cross-relaxation has yet to be observed in PCF, limiting efficiencies to less than 40 %.

Energy up-conversion is nearly opposite to cross-relaxation. In this case, a signal photon is transferred to an already excited ion promoting it to a higher state [63]. This energy transfer can become dominant for very small ion-ion separations, leading to increased thresholds and low slope efficiencies if clustering isn't prevented. Therefore, optimal co-doping concentrations are crucial in thulium-doped fiber design to prevent clustering, for maximizing cross-relaxation while minimizing energy up-conversion [68].

2.4.2 Applications at 2 μm

One interesting application exploiting thulium's large gain bandwidth is atmospheric sensing and ranging. Within the 1.7 – 2.1 μm region, there is both high atmospheric transmission as well as water and CO_2 absorption [69]. By utilizing a tunable wavelength source [70], both these applications could be harnessed [71, 72]. Thulium fiber lasers have also shown promise in medicine, such as for fragmenting urinary stones [73].

Working at longer wavelengths, such as 2 μm, provides an advantage for generating mid-infrared light. Thulium fiber lasers offer an efficient high peak power platform for directly pumping an optical parametric oscillator, such as $ZnGeP_2$ [74, 75]. These platforms also enable all-fiber, compact sources for supercontinuum generation [76]. Because silica fibers have a ~2.5 μm absorption edge, different glass compositions allow supercontinuum extending to 4 μm, such as chalcogenide [77].

For scaling USP peak powers, it will be shown in Chapter 3 that some nonlinear effects scale inversely with wavelength. Therefore, by operating at a longer wavelength, these nonlinear effects are mitigated relative to a 1 μm counterpart. This is one major inherent advantage of working with thulium. Another is seen by Equation 3, in which longer wavelengths allow single-mode operation for larger core diameters.

CHAPTER 3: LIMITATIONS FOR SCALING PEAK POWERS

The generation and amplification of USP to high peak powers has enabled the study of many interesting nonlinear effects (NLE). However, when amplifying USP, NLE distort the pulse spectrum and leads to degradation of pulse quality. To produce transform-limited, high quality pulses, NLE need to be mitigated. The onset and strength of these NLE highly depend on the optical intensity and interaction length. Because of this, USP fiber amplifiers suffer the most due to their tightly confined MFA and long guidance. Hence, main limitations in scaling peak powers in fiber systems is largely due to NLE, with some bottlenecks also arising from fiber damage and thermal effects [78, 79]. In the 3 MW USP system, pulse quality was degraded due to multimode interference (MMI), but has potential for further peak power scaling before the onset of NLE [8].

In this chapter, four limiting NLE are described in section 3.1, and are related to the third-order susceptibility, $\chi^{(3)}$. These NLE can be grouped into two categories: those arising from the Kerr effect such as self-focusing and self-phase modulation (SPM); and those arising from inelastic scattering such as stimulated Raman scattering (SRS) and stimulated Brillouin scattering (SBS). Section 3.2 introduces MMI and its effect on pulse quality, which degraded the 3 MW USP system. Lastly, section 3.3 reviews record peak power systems and their approach at mitigating the onset of NLE.

3.1 Nonlinear Effects

3.1.1 Self-focusing

As light propagates through a medium, it has been shown that the refractive index is modified by the light's intensity, known as the Kerr effect [9, 80]. This can been seen in Equation 5, where n_2 is the nonlinear index with units of m^2/W.

$$n(r) = n + n_2 I(r) \quad (5)$$

Most materials exhibit positive n_2 values, such as silica. Thus, for a fiber's fundamental mode, the center of the beam experiences a larger refractive index than the outside. This causes a positive lensing effect, known as self-focusing. Equation 6 shows that at a critical peak power, P_c, the lensing effect overcomes diffraction and causes the beam to collapse on itself.

$$P_c = \alpha \left(\frac{\lambda^2}{4\pi n n_2}\right) \quad (6)$$

In this formula, α is a constant found to be ~1.8 – 2.0 [81]. For linearly polarized light in silica fibers, this theoretical critical power is ~4 MW at 1 μm, and ~16 MW at 2 μm ($n_2 \cong 2.7 \times 10^{-20}$ m^2/W [82]). Peak powers > 5 MW have been reported in a sub-nanosecond system utilizing an 80 μm core Yb:PCF amplifier [83]. At these pulse durations the nonlinear index decreases allowing theoretical peak powers in the 5 – 6 MW range. Nonetheless, the self-focusing effect enforces a limiting peak power inside a solid-core fiber, and can only be mitigated by working at longer wavelengths, such as 2 μm. Future directions to surpass this limit are hollow core fibers to maintain benefits of fiber delivery, while reducing the nonlinear index by propagating in air [81, 84].

3.1.2 Self-phase Modulation

While self-focusing was the spatial result to the Kerr effect, SPM is the temporal analog [85, 86]. The additional phase shift the pulse, with power P_0, encounters due to the Kerr effect across length L_{eff} is shown in Equation 7.

$$\Phi_{SPM} = n_2 I(r) \cdot k_0 L_{eff} = \frac{2\pi}{\lambda} \frac{n_2}{\mathrm{MFA}} L_{eff} P_0 \qquad (7)$$

As the pulse passes through the medium, the frontside will experience an increase in instantaneous frequency while the backside experiences a decrease. This will result in the pulse's bandwidth spreading, due to the generation of additional frequencies. If the power is continually scaled, peaks and dips in the optical spectrum occur due to constructive and destructive interference between identical frequencies. These spectrum degradations affect pulse quality and are unwanted.

As seen in Equation 7, alleviating SPM onset can be accomplished experimentally be either reducing fiber length or increased MFA. The former is not reasonable when high gain is desired, and the latter is being applied by movement towards PCF with large MFA. Additionally, working at 2 μm relieves the onset of SPM by the inverse proportionality to wavelength.

3.1.3 Stimulated Raman Scattering

When light scatters from a particle, it typically leaves with the same energy as it started, known as Rayleigh scattering (elastic scattering). However, very rarely the energy for the scattered light will be smaller, or larger, than it started. This shift in energy is due to the vibrational or rotational energy of the particle the light scattered from. For solid materials such as silica fibers, it is due to vibrational energies, $\hbar\omega_{vib}$ [87]. This occasion is known as spontaneous Raman scattering (inelastic

scattering). Figure 6 shows a Jablonski diagram for these processes. A Stokes shift corresponds to light, E_s, losing energy to the vibrational energy of the molecule, and anti-Stokes shift being the opposite. A Stokes shift is more probable than anti-Stokes.

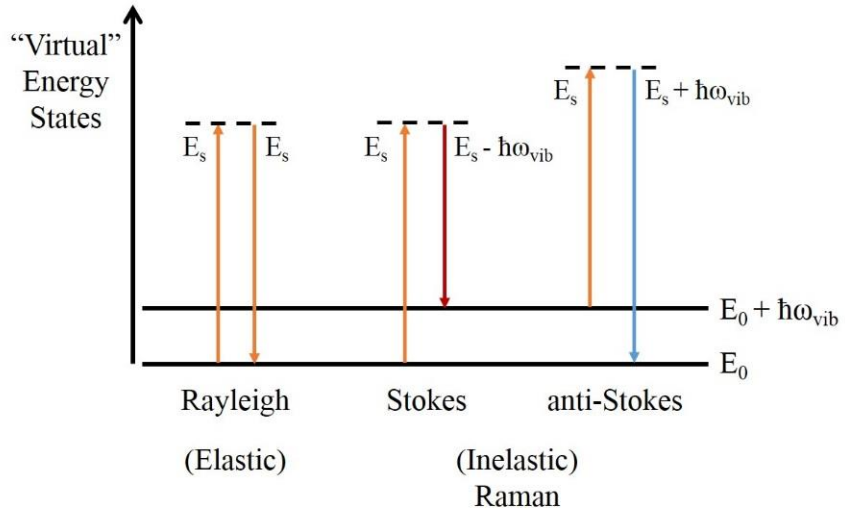

Figure 6. Jablonski diagram for Rayleigh and Raman scattering.

If the input signal is sufficiently powerful, and the interaction length is long (such as in a fiber), then the spontaneous Raman shifted light can become a seed and experience amplification. This is known as stimulated Raman scattering (SRS), and shifts the laser signal to a different frequency disrupting the optical spectrum. In silica, the frequency shift is maximum at ~13 THz [86]. For CW lasing, the threshold input power for when the forward propagating Stokes wave is equal to the signal wave's output power is given by Equation 8, where g_R is the Raman-gain coefficient [86].

$$P_{th}^{SRS} \approx \frac{16\,\mathrm{MFA}}{g_R L_{eff}} \qquad (8)$$

For USP, this approximation begins to break down due to group velocity dispersion and pump/signal walk-off [86]. For pulses < 100 femtoseconds, SRS analysis becomes even more complicated because the pulse duration is the same order of magnitude as the Raman response time. However, Equation 8 still highlights key factors to increase SRS threshold. Reducing interaction length and increasing MFA, such as in PCF, will alleviate SRS symptoms. Also, g_R is inversely proportional to wavelength, so increasing wavelength consequently increases the threshold, another benefit for working at 2 μm.

Lastly, an important effect in USP systems is intrapulse Raman scattering [86]. Because of the USP large bandwidth, the high frequency components can transfer energy to the low frequency components. This will redshift the pulse's spectrum and has applications in Raman soliton self-frequency shift (SSFS) amplifiers for tuning output wavelengths [88], which is exploited in the 3 MW system [8, 89].

3.1.4 Stimulated Brillouin Scattering

While SRS dealt with inelastic scattering from vibrational modes, SBS is inelastic scattering from low frequency acoustic modes. The signal wave induces density fluctuations in the fiber from electrostriction, producing a refractive index grating. This grating causes Bragg diffraction, and in contrast to SRS, the scattering for SBS occurs in the backward direction reflecting the signal power. This effectively limits forward output power. As with SRS, a similar analysis can be carried out producing Equation 9. This shows the threshold power for when Brillouin scattering becomes stimulated in a CW laser, where g_B is the Brillouin-gain coefficient [86].

$$P_{th}^{SBS} \approx \frac{21 \text{ MFA}}{g_B L_{eff}} \quad (9)$$

Because SBS in silica fibers has a narrow gain bandwidth of ~10's MHz, USP rarely suffer from SBS because of their large bandwidth. SBS is a major limiting factor in single-frequency amplifiers. For low repetition rate (<10 MHz) USP systems, effects from SBS essentially cease to occur because the signal pulse duration is much shorter than the acoustic lifetime, which is ~10's nanoseconds [86]. Nonetheless, mitigating SBS is accomplished using the same methods as SRS, by increasing MFA and decreasing effective length. Furthermore, SRS has a lower threshold and is more prevalent for USP systems.

3.2 Multimode Interference

To mitigate the aforementioned NLE as well as fiber damage, scaling the fiber diameter is an often used solution. However, as you increase fiber core diameters, the waveguide will begin to support HOM. Methods to minimize HOM content were discussed in section 2.2.3 and section 2.3.

If a fiber that supports few HOM is used as a final power amplifier, inevitably some power will be located in this HOM content. Typically, the power distribution is optimized where the HOM would be negligible and not considered of any importance. However, in USP, this can ultimately affect pulse spectrum and compressed pulse quality due to MMI.

MMI occurs because different transverse modes propagate at different velocities, due to differences in effective index [11]. For example, if there are two modes excited in a fiber, these two modes will propagate with a group delay difference dependent on the difference in propagation speed, and on fiber length. Because the two modes are coherent and propagating in the same

waveguide, they interfere constructively or destructively at each wavelength dependent on the relative phase at the measured location. This will produce peaks and valleys in a broadband optical spectrum. These spectral modulations are used for measuring HOM content via S^2-analysis [90].

Fundamentally, a broad spectrum is required in order to produce USP. Therefore, if MMI occurs during amplification of an USP, the optical spectrum becomes distorted due to these peaks and valleys. The spectrum is no longer transform-limited because of these modulations. Compressing the pulse will result in sub-optimal pulse duration, and satellite pulses that remove useful energy from the main pulse. This will limit achievable pulse durations and peak powers in USP if not prevented. As anticipated, this is undesirable and single-transverse-mode beam quality is preferred prior to amplification and pulse compression.

3.3 Recent Progress in Scaling Peak Powers

Due to ytterbium's simple energy level structure and small quantum defect, the majority of high power fiber lasers are ytterbium doped. Nonetheless, scaling peak powers in these systems face similar difficulties to thulium doped lasers, namely NLE and fiber damage [23]. The two straightforward solutions to mitigate NLE are increasing the pulse's spatial and temporal parameters to reduce the optical intensity. This is accomplished by increasing the fiber's MFA and spreading the pulse duration. The former method was discussed in Chapter 2, and the latter method is routinely performed by chirped pulse amplification (CPA) [91]. In this technique, a dispersive element first increases the pulse duration prior to amplification. This consequently reduces the peak power reached in the fiber during amplification. The amplified output pulse is then

compressed via the opposite dispersion used to stretch it, resulting in high peak power, ultrashort pulses. Figure 7 graphically demonstrates this approach.

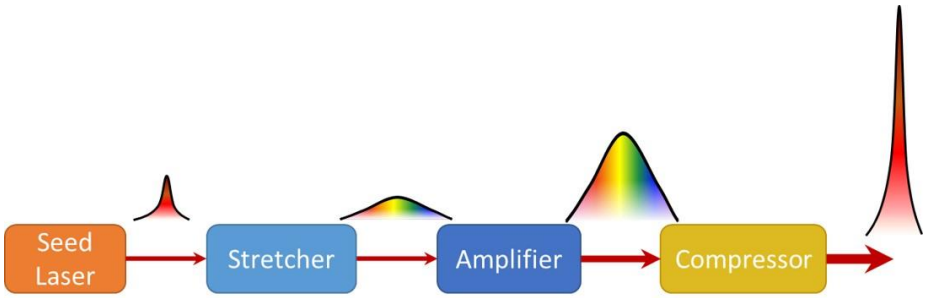

Figure 7. Graphical demonstration of CPA.

For ytterbium-doped fiber systems, [92] reported peak powers of 2.5 MW in 2003 using CPA and LMA Yb:SIF with MFA of 415 μm^2. Because the large SIF supported HOM, bend losses had to be introduced, but still enabled nearly single-mode beam quality with $M^2 \sim 1.1$ [92]. The same group then utilized a PCF amplifier in 2005, increasing peak power outputs to 8.2 MW with over 100 W average power [93]. This Yb:PCF had MFA of ~1000 μm^2 and provided single-mode beam quality with $M^2 < 1.2$. In 2007, ~1 GW peak powers were produced using a similar technique, but employing a ~4000 μm^2 MFA Yb:PCF to reduce onset of NLE [50]. At the highest output, satellite pulses were observed due to SPM. Lastly, the record peak power of 3.8 GW was accomplished in 2011 [56]. This required incorporating a spatial light modulator to actively control the pulse's phase, and a 8600 μm^2 MFA Yb:LPF for the final stage amplifier. Further power scaling was believed to be limited by mode-anticrossing [56].

A downside to the systems discussed is the need for free-space grating compressors, as well as the rigid rod-PCF. These ruin the compact advantages of fiber architecture, requiring large spatial

footprints for free-space compressors and non-bendable fibers. However, these drastic improvements (peak power increase of 1500-fold in 8 years, seen in Figure 8) are demonstrating that fiber-based systems can compete, and will eventually rival, bulk solid-state media.

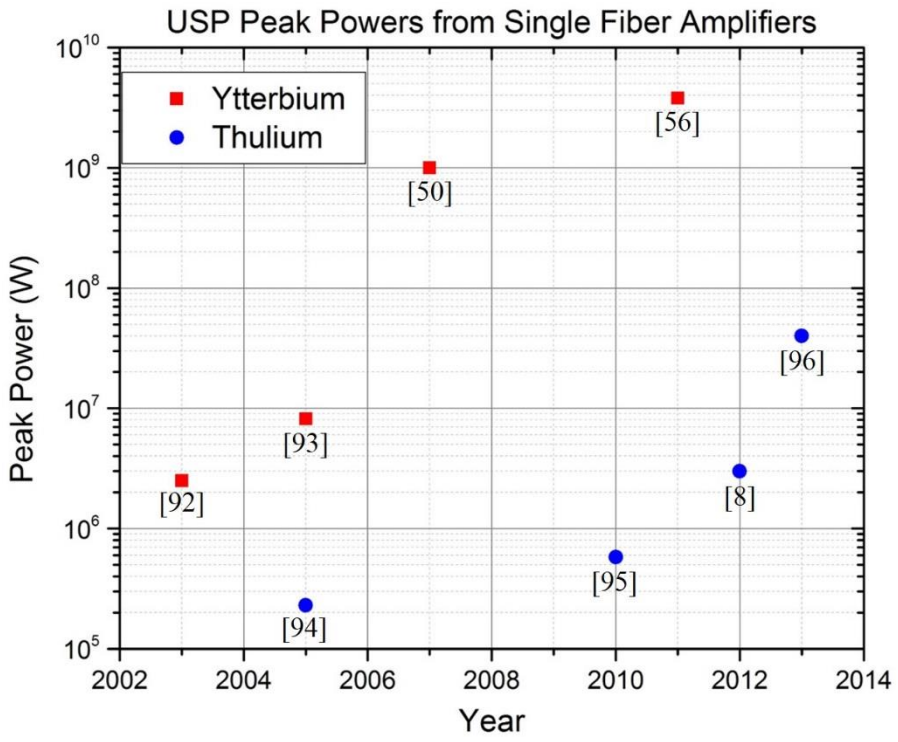

Figure 8. Historical peak powers from USP, single fiber amplifiers [8, 50, 56, 92-96]

Thulium-doped fiber lasers are beginning to see a similar rise in performance as with the ytterbium-doped counterparts. Main disadvantages with thulium are the increased heat load, and immature fiberized components at 2 μm. However, these are being addressed and higher peak powers are still practical. 2005 saw the first demonstration of a high peak power thulium-doped system, using a Raman-shifted Er:Yb oscillator and amplifying in Tm:SIF to produce 230 kW peak power without an external free-space grating compressor [94]. This system utilized a 25 μm core diameter Tm:SIF with MFA ~ 400 μm^2 as the power amplifier. This specific fiber, developed by

Nufern [97], will be used as the final amplifier for all the following systems described, and is commonly used in high-power thulium-doped systems. In 2010, CPA was introduced after amplification of a thulium-fiber oscillator to compress the pulse duration, boosting peak powers to ~580 kW [95]. In 2013, the custom-built system described in section 5.1 demonstrated >3 MW peak power by reducing the repetition rate and utilizing CPA as well [8]. At the highest powers, MMI degraded pulse quality impeding further scaling. PolarOnyx later demonstrated peak powers of ~40 MW using a comparable system to our design [96]. They observed spectral broadening attributed to Raman scattering, and believe the output could be potentially doubled with additional pump power. Overall, USP thulium fiber lasers have seen a factor of 150-fold increase in peak power over the past 8 years, seen in Figure 8.

In contrast with ytterbium systems, the mentioned USP thulium systems have yet to incorporate novel PCF fiber designs to scale MFA. In the nanosecond regime, utilizing Tm:PCF as a final amplifier produced record peak powers of ~1 MW [58]. Similar PCF designs can be integrated into USP systems, potentially scaling peak powers to GW-levels. As mentioned previously, thulium's 2 μm emission inherently mitigates some NLE compared to 1 μm. Thus, peak powers in thulium systems could potentially outperform ytterbium systems in the future.

A final comment on power scalability is that these GW-level record peak powers still fall short of TW bulk solid-state systems. Single fiber amplifiers inherently have limits, requiring new methods to reach extreme peak powers for high-intensity physics experiments. One method, routinely used in CW systems, is beam combining. For USP, this requires active phase control, and has already been demonstrated using four Yb:LPF producing 1.8 GW peak power, 530 W average power, and

excellent beam quality of $M^2 \sim 1.2$ [98]. Another method is divided-pulse amplification, in which the pulses are delayed temporally and amplified in the same fiber [99]. Combining these two methods could produce fiber CPA systems with TW-level peak powers and kW-level average powers.

CHAPTER 4: "ALL-FIBER" LASER SYSTEMS

The end goal for fiber laser design is to achieve an "all-fiber" setup that removes free-space components. The telecommunication boom, occurring at 1.55 μm, pioneered this effort for erbium-doped fibers. However, mature fiberized components at wavelengths such as 2 μm are still being developed, including their power handling capacity. Section 4.1 will overview the required components and recent development for these component at 2 μm. Section 4.1.1 will detail fiber pump combiners, due to their relation to the experimental work in Chapter 5. Lastly, section 4.2 will highlight some recent systems incorporating these elements for an "all-fiber" layout.

4.1 Fiber Components

The minimum components needed to produce a fiber laser can be seen in Figure 9. This shows free-space coupling through dichroic mirrors that provide pump input as well as signal feedback. This configuration is not optimal because coupling into a 5-25 μm diameter fiber core is susceptible to environmental effects and is not easily packaged.

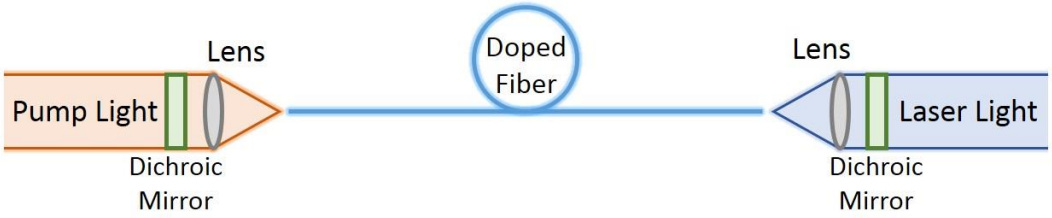

Figure 9. Basic, free-space, fiber laser schematic.

To facilitate "all-fiber" laser architecture, there are three key components: pump combiner, fiber Bragg grating (FBG), and fiber isolator. The pump combiner removes the necessity for dichroic

mirrors, and enables a fiberized method to inject pump light. This component is discussed in section 4.1.1. The FBG acts as the signal feedback, and manufacturing conditions can produce a high- or low-reflectivity FBG at the desired wavelength, depending on the usage [100]. Isolators are imperative to prevent feedback into the cavity, and isolators can actually be produced inside the fiber itself [101, 102], with a commercial product available [103]. Some additional fiber components that are useful and/or depend on the fiber design and application are: mode-field adaptors, splitters, circulators, chirped FBGs, saturable absorbers, etc. Figure 10 shows a fiberized laser system, highlighting no free-space coupling and the inherently compact design.

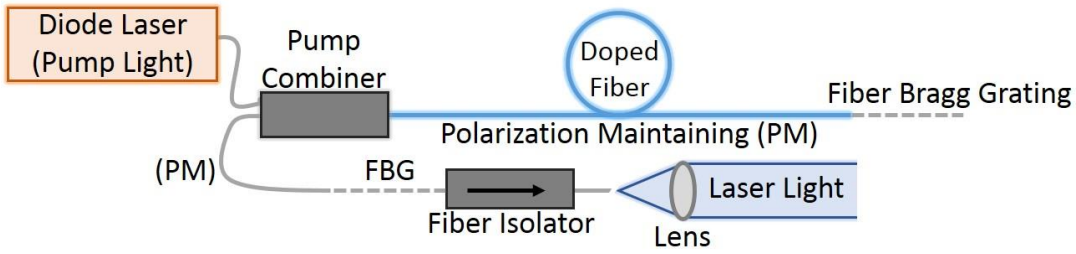

Figure 10. Fiber laser system utilizing "all-fiber" components.

Specifically, fiber isolators at the 2 μm regime have just recently become commercially available. High power handling with low insertion loss and high isolation is challenging in this regime, especially if attempting to cover thulium's broad bandwidth. A handful of companies produce 2 μm isolators, such as Thorlabs [104], AdValue Photonics [105], and Shinkosha [106]. In the past couple of years, specifications have improved and typical power handling capacities are 5-10 W. Isolations and PER greater than 30 dB are now available, however with a larger cost compared to 1-1.55 μm products.

FBGs allow an all-fiber mirror and output coupler for laser construction. Many companies produce these, although very few openly supply them at 2 μm, such as TeraXion [107], ITF Labs [108], and O/E Land, Inc. [109]. It is likely that companies specializing in FBG design would collaborate with a group requiring special wavelength considerations. Nevertheless, typical reflection bandwidths are ~5 nm or less, and broadening this would be useful for USP systems or miscellaneous applications.

Another vital component for fiber lasers are mode-field adaptors (MA). These components modify the beam's MFA. An example is transferring from a 10 μm to 25 μm fiber core diameter, typically found when coupling from low-power oscillators to high-power amplifiers. A common method to produce this is via tapering, where the fiber is heated and stretched to adiabatically shrink the core-to-cladding ratio [110]. Considerations imperative to MA design are power conservation, maintaining single-mode quality, maintaining polarization if PM, and high power handling capacity. The tapering routine can typically be done in-house, leading to robust, low-loss MA after optimizing the tapering routine. There are many suppliers for high-power MAs, and it is likely any could produce them for 2 μm on request. ITF Labs is the company used in our custom-built thulium-doped system [89, 111].

4.1.1 Fiber Pump Combiners

Components that enable all-fiber pump coupling with high power thresholds are crucial for fiber laser development [112]. These technologies typically use fused tapered fiber bundles (TFB) to combine multiple pump sources into one output fiber [113, 114]. TFB are produced by arranging N fibers in a close-packed structure around a central fiber, to produce circular symmetry. Then,

the fiber bundle is heated to fuse the fibers, and then tapered to a final dimension dependent on the application. These are denoted by (N + M):1, where N is the number of pump fibers, M the number of signal throughput fibers, and :1 denoting that one fiber is the resultant output. Figure 11 shows a diagram and facet profile schematic for a (6+1):1 combiner.

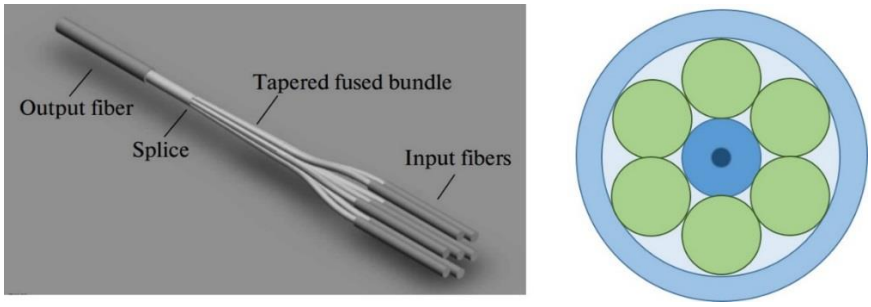

Figure 11. Left: Diagram of how a TFB is implemented [115]. Right: Facet profile schematic for a (6+1):1 bundle with surrounding capillary.

While the design for TFB may seem simple; efficient and robust manufacturing routines are required to produce efficient pump coupling and brightness conservation through the component. Even just 90 % coupling efficiency for a multi-kW pump combiner generates 100's watts of heat dissipated in a localized region. Therefore, efficient thermal packaging is just as important as producing the TFB.

Nonetheless, commercial pump combiners are available, and are rated for > 1 kW performance [116-118]. Signal combiners with 4 kW power handling capabilities have also been reported [119]. While the TFB allows all-fiber integration for laser oscillators and amplifiers, it doesn't permit easy integration for complicated designs such as PCF. A new class of pump combiners utilizing PCF are now being investigated, one of which is detailed in section 5.2 and characterized in section 5.3.

4.2 "All-fiber" 2 μm Systems

With the recent progress in fiberized components, systems operating in CW, nanosecond, picosecond, and femtosecond regimes have already been developed that exploit the "all-fiber" concept at 2 μm. Notably, the CW record output power of 1 kW was accomplished utilizing a simple all-fiber MOPA architecture with two amplifier stages [120]. In the nanosecond regime, a gain-switched 1.55 μm seed diode with a fiberized output pumped a thulium amplifier to produce 8 W of average power, 35 μJ pulse energy, and 25 nanosecond pulse durations in a polarized "all-fiber" format [121]. The picosecond regime saw a similar design by utilizing a 2 μm gain-switched diode as the seed for amplification in all-fiber Tm:SIF [122]. The final LMA Tm:SIF amplifier was pumped via free-space coupling, but incorporating an all-fiber pump combiner would be feasible. Nonetheless, record peak powers of 100 kW were achieved in this 2 μm picosecond system.

Mode-locking 2 μm femtosecond pulses in an all-fiber format has been accomplished in many ways as well. The first thulium-doped figure-eight laser was all-fiber and permitted output pulse durations from 100 picoseconds to 20 nanoseconds [123]. This also used an all-fiber amplifier to generate 50 nJ pulses compressed at 370 femtoseconds. A carbon nanotube saturable absorber was used in [124] to generate ~1 picosecond output pulses, and then by stretching a fiber taper, the output was wavelength-tunable over 50 nm. These two cases are of interest for their tunable pulse durations and center wavelengths. Another method for producing all-fiber femtosecond pulses is nonlinear polarization evolution, as in [125]. Overall, several papers have reported all-fiber 2 μm ultrashort pulse generation, including the custom-built system described in section 5.1.

CHAPTER 5: CHARACTERIZATION OF A PCF PUMP COMBINER FOR POTENTIAL USP AMPLIFICATION

From Chapter 2, PCFs were introduced that demonstrated huge advancements in scaling MFA while remaining essentially single-mode. This consequently decreases the optical intensity in the fiber during amplification, mitigating NLE as discussed in Chapter 3. Namely, their improved single-mode guidance over SIF make them attractive to minimize MMI, which was the limiting factor for further peak power scaling in the custom-built, 3 MW, thulium-doped USP fiber system. In this Chapter, we investigate the performance of an integrated component that incorporates a Tm:PCF amplifier and pump combiner to further increase peak powers. The component's architecture is also all-fiber, simultaneously enabling the benefits for an "all-fiber" system as discussed in Chapter 4.

To provide an example of MMI and the limitations this can pose during amplification, section 5.1 overviews the 3 MW USP system. The final Tm:SIF amplifier is deemed inadequate and section 5.2 presents a pump combiner that incorporates PCF geometry. This pump combiner is spliced to Tm:PCF to form an amplifier, and is characterized in section 5.3 using a CW source. In section 5.4, it is concluded that the component is suitable for USP amplification, but needs further optimization to enable higher optical-to-optical efficiencies.

5.1 3 MW, sub-500 Femtosecond, Thulium-doped Fiber Laser

Before the PCF pump combiner is detailed, it would be useful to first overview the 3 MW system in which MMI occurred. Dr. R. Andrew Sims constructed the system as part of his PhD dissertation, and the front-end comprises a soliton mode-locked (ML) oscillator, which is coupled

into a Raman SSFS amplifier to broaden and smooth the spectrum. This output is temporally stretched via a chirped Bragg grating (CBG) and sent through a pulse picker reducing the repetition rate. It is subsequently amplified and compressed to 3 MW peak power [8, 89].

In detail, the oscillator entails a carbon nanotube saturable absorber that initiates ML [126]. Because 2 μm falls in the anomalous dispersion regime in the fiber, the pulses ML in the soliton regime, in which the Kerr effect balances dispersion to produce stable pulses [127]. Figure 12 shows the all-fiber oscillator schematic and a typical output spectrum, exhibiting Kelly sidebands which are typical for soliton ML fiber oscillators [128]. Polarization controllers were used to help ensure stable ML assisted by nonlinear polarization evolution [129].

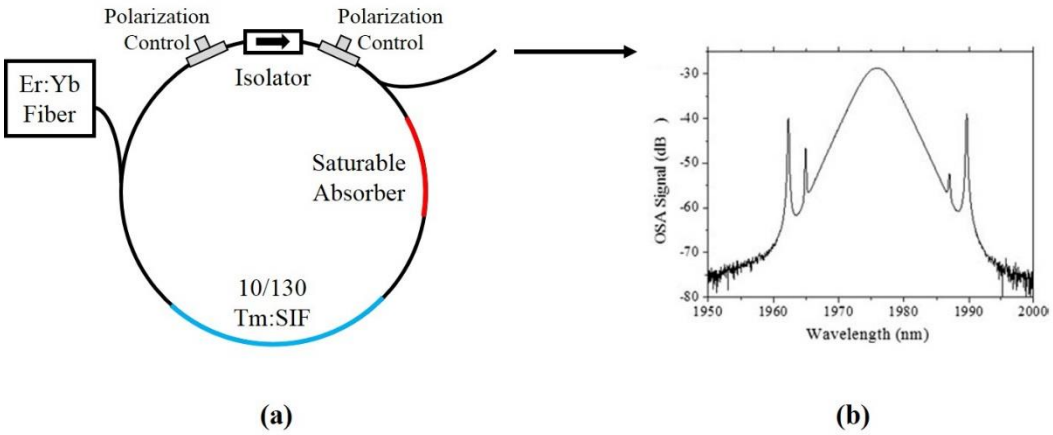

Figure 12. (a) 3 MW system's soliton ML oscillator. (b) Typical spectrum for the oscillator, exhibiting Kelly sidebands [89].

The output pulses had a 5 nm spectral bandwidth centered at 1975 nm with a 60 MHz repetition rate. This was free-space coupled through an isolator into a Raman SSFS amplifier to smooth the spectrum of the Kelly sidebands and shifts the center wavelength to 2020 nm. This Raman SSFS

amplifier also broadens the bandwidth to produce transform-limited 150 fs pulses. To promote CPA, a CBG is then used to chirp the pulses to ~160 ps. Figure 13 shows a Raman SSFS pulse overlaid on top of the CBG reflectance window.

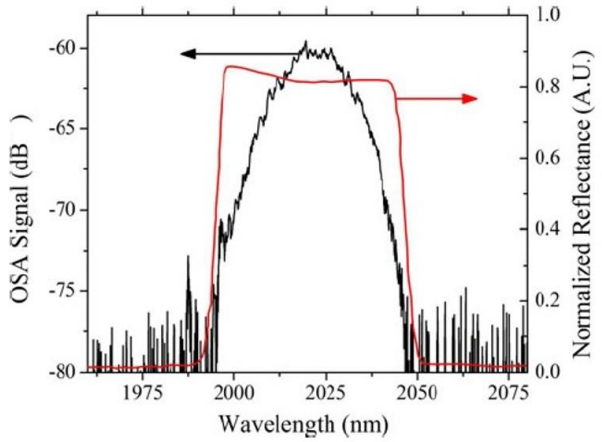

Figure 13. Spectrum of the pulse reflecting off the CBG, and the CBG's reflectance window [89].

These chirped pulses were amplified in a 10/130 Tm:SIF prior to reducing the repetition rate to 100 kHz with an electro-optic modulator, and then re-amplified in a 10/130 Tm:SIF. Lastly, a 25/400 LMA Tm:SIF amplifier is used to promote ~3 MW peak powers after compression using free-space diffraction gratings [8]. The simplified schematic can be seen in Figure 14.

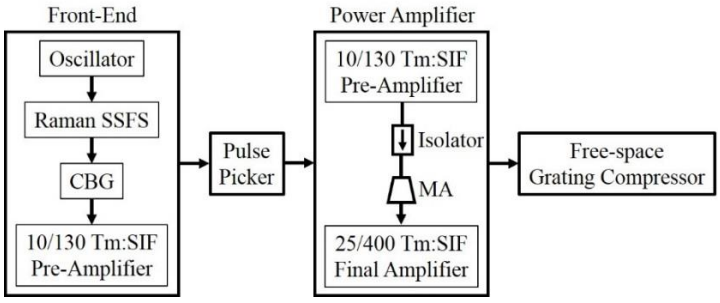

Figure 14. 3 MW system's schematic; CBG: chirped Bragg grating, MA: mode-field adaptor.

The compressed output pulses show satellite pulses in the autocorrelation, with 1 μJ confined to the central 500 fs region, seen in Figure 15. The degraded pulse quality is due primarily to MMI. Pulse spectra were taken at several points surrounding the LMA Tm:SIF amplifier, also shown in Figure 15. This clearly shows that MMI (spectral modulations) was first initiated by the fiber splices and MA, and significantly magnified during amplification in the LMA Tm:SIF.

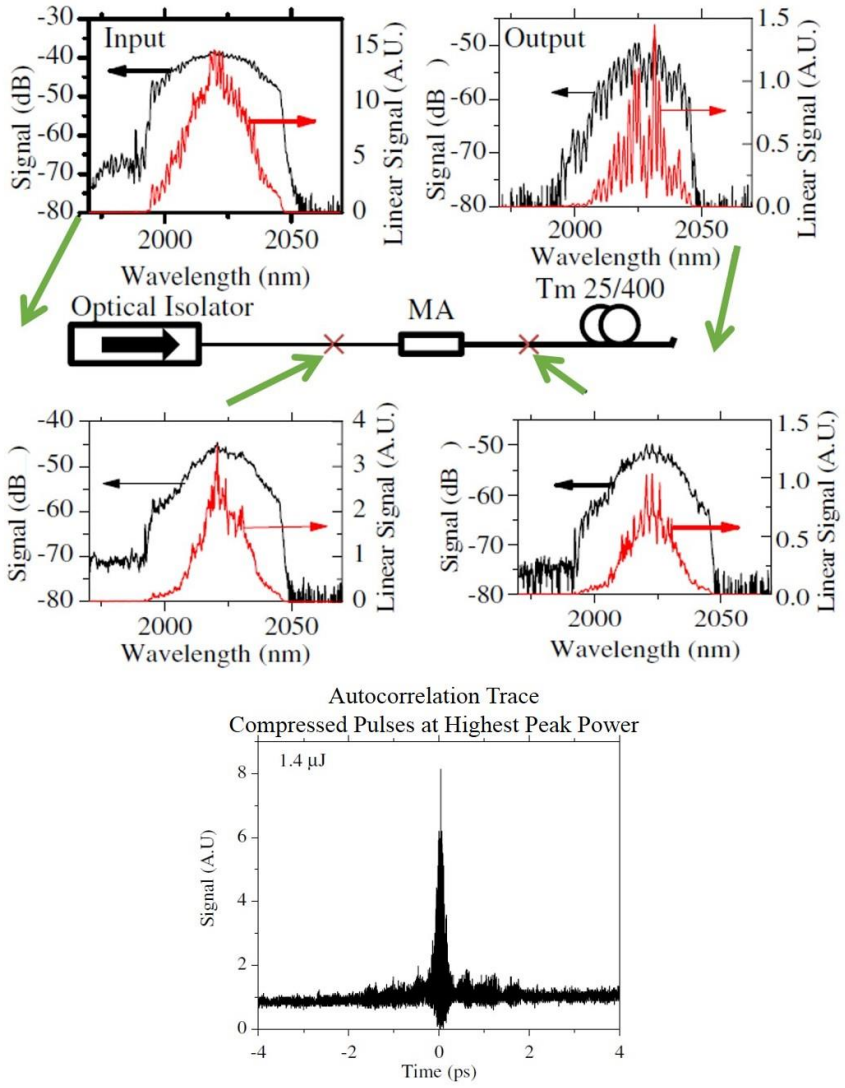

Figure 15. Top: Spectra at various points around the LMA Tm:SIF amplifier. MMI occurs after the MA and is further aggravated with amplification. Bottom: Autocorrelation trace [8].

These spectral oscillations that cover the frequency envelope produce satellite pulses in time, offset from the central pulse. This is because frequency/time are related by the Fourier transform. Thus, it is necessary to mitigate MMI. PCF meets this requirement while simultaneously providing large MFA. In the next section, we introduce an integrated pump combiner that incorporates a MA from SIF to PCF for incorporation into an all-fiber amplifier.

5.2 Integrated PCF Pump Combiner

As discussed in section 4.1.1, pump combiners based on step-index profiles are commercially available and permit power scalable, all-fiber systems. New approaches to include PCF designs are imperative for promoting single-mode, low nonlinearity, high power amplifiers. However, PCF's microstructured design and air holes make all-fiber integration complicated. Conventional splicing techniques collapse the air holes during heating, destroying the waveguide structure. Directly splicing SIF to PCF leads to high transmission losses, requiring specialized techniques and optimized splicing routines to minimize loss.

Several papers have been presented at conferences detailing pump combiners that incorporate PCF architecture since 2007 [130-132]. The pump combiner investigated in this work was manufactured by Optical Engines, Inc. The design consists of three stages: a fiber bundle containing the signal SIF and multimode pump fibers, a combining fiber that maintains core dimensions with an adiabatically etched taper that reduces cladding dimensions to match the PCF pump cladding, and the output PCF fiber. All three stages are spliced together. A pump combiner utilizing this design was first described in 2010 [133]. Figure 16 shows a schematic of the combiner architecture.

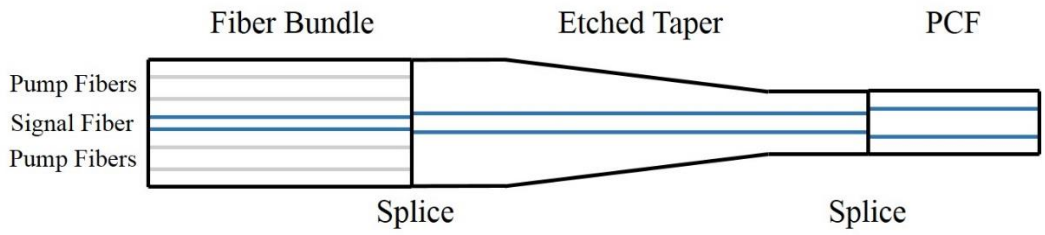

Figure 16. Typical PCF pump combiner architecture.

Important design considerations for constructing such combiners entail maintaining pump guidance and brightness while transferring from the SIF bundle to PCF output. Highly optimized routines have produced these pump combiners operating at ~92 % pump transmission, with the majority of losses occurring at the tapered fiber to PCF splice [134]. Optical Engines, Inc. create a cladding mode stripper at the taper to PCF splice to remove this uncoupled light. This is accomplished by etching a portion of the PCF after the splice.

For high power operations, such as the 1.5 kW of pump power in [134], this still produces 100's of watts of heat dissipated into a localized region. A specialized package for the combiner was developed to remove this heat, and Figure 17 shows that the highest temperatures reached in a similar combiner was 104 °C, which is far below the 260 °C limit for the silicon used to secure the fiber. Nevertheless, Optical Engines, Inc. is developing further iterations of packaging to handle higher heat loads, for further pump power scaling.

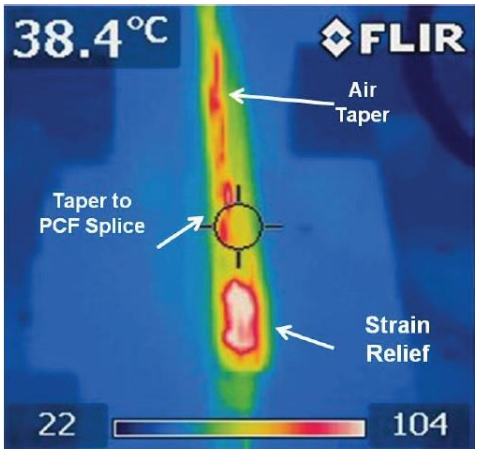

Figure 17. Thermal image of a similar combiner at 1.5 kW pump power [134].

Optical Engines fabricated a similar set of pump combiners utilizing Tm:PCF, and this work describes some of the initial characterization of the amplifier performance at 2 μm. The specifications for this pump combiner are as follows, with mode-field/cladding diameters listed in microns: fiber bundle containing one PM-SIF 24/250, 0.06 NA signal input and nine 105/125, 0.22 NA multimode pump fibers, which is spliced to a non-PM 32/480 SIF etched to match the pump cladding diameter of a 39/250, 0.06 signal NA passive PM-DC-PCF. These are the calculated mode-field diameters at 1932 nm. The taper fiber is non-PM because it is held rigidly straight, thus polarization should be maintained throughout. Figure 18 shows facet images for the signal input and a similar passive PCF output.

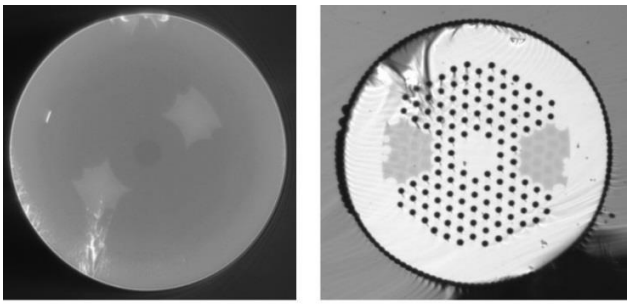

Figure 18. (a) 25/250 signal input facet. (b) 50/250 passive PCF facet (the pump combiner was purchased pre-spliced to Tm:PCF, this image is of a typical passive PCF matched for Tm:PCF from NKT Photonics).

At the time of purchase, Optical Engines, Inc. did not have a 2 μm source, so the signal coupling was measured at 1.55 μm, pump coupling was measured with fiber-coupled laser diodes at 980 nm and 0.22 NA. Actual operating conditions would be signal coupling at ~1985 nm and pump coupling at ~790 nm. The tested power loss and estimated transmission efficiency is seen in Table 1.

Table 1. Loss specifications for PCF pump combiner.

Port	* Loss (dB)	Estimated Transmission (%)
Pump 1	0.12	97.3
Pump 2	0.13	97.1
Pump 3	0.15	96.6
Pump 4	0.15	96.6
Pump 5	0.14	96.8
Pump 6	0.13	97.1
Pump 7	0.17	96.2
Pump 8	0.13	97.1
Pump 9	0.16	96.4
Signal **	1.7	67.6
* As tested with a 980 nm fiber-coupled laser diode at 0.22 NA ** Signal loss and PER measured at 1.55 μm. Signal PER > 20 dB		

Overall, a similar integrated step-index to PCF pump combiner was demonstrated with a Yb:PCF amplifier, producing ~1 kW output powers [134, 135].

5.3 CW Characterization of an Integrated, All-fiber, Tm:PCF Amplifier

In order to produce a laser amplifier, Optical Engines spliced the pump combiner to ~3 meters of Tm:PCF, which was fabricated by NKT Photonics. The output facet was fused to prevent air-hole contamination, and then cleaved at ~4.5° angle to prevent parasitic lasing, and. The PCF-Tm:PCF splice was mounted and secured in a heat sink similar to the heat sink used for the pump combiner. Figure 19 shows pictures of the initial set-up used for housing and cooling the integrated Tm:PCF amplifier, a simplified schematic, and the Tm:PCF output facet.

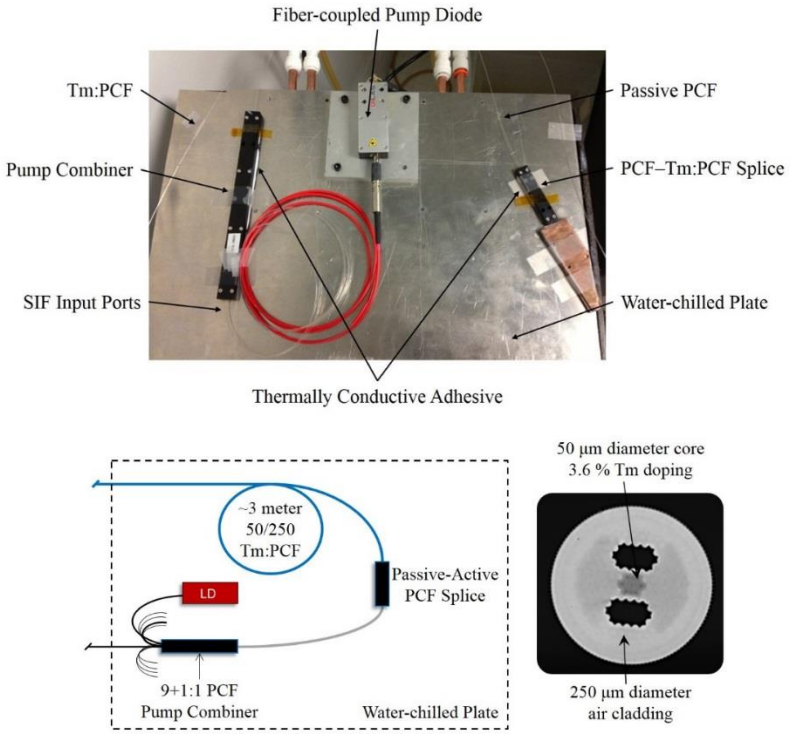

Figure 19. Top: Picture of initial set-up for the PCF pump combiner. Bottom: Schematic for the Tm:PCF amplifier and image of Tm:PCF output facet.

The characterization was performed in two parts, both with CW seeds. First, a 25 mW broadband amplified spontaneous emission (ASE) source was used to investigate the gain bandwidth and spectral quality of the integrated amplifier. Second, a 650 mW laser seed was used to investigate the slope efficiency, beam profile/quality, and polarization properties of the integrated amplifier. All of these tests will be summarized and concluded in section 5.4 in relation to prospective use as an USP amplifier.

5.3.1 Characterization using ASE Seed

For transform-limited $sech^2$-shaped USP (as generated in the 3 MW system's oscillator), a spectral full-width half-maximum of at least 8 nm is required to achieve 500 fs pulses, and 40 nm is required for 100 fs pulses (at a center wavelength of 1950 nm). If the amplifier's gain bandwidth is too narrow, gain narrowing can occur. In this scenario, the spectral content of the pulse correlating to the amplifier's gain maximum experiences more gain than the wings, effectively decreasing spectral width. This can limit the achievable output pulse duration. Thulium is known for possessing a large gain bandwidth as mentioned in section 2.4, and a broadband ASE source was utilized to test the amplification bandwidth of the integrated PCF amplifier.

The ASE source was constructed by splicing a 35 W, 79x nm pump diode (DILAS) to a 2+1:1 PM-SIF pump combiner (ITF Labs). Because this system is designed to be an ASE source, the pump diode was spliced in the counter-propagating configuration to enable higher ASE powers compared to co-propagating. The signal output was spliced to ~2 meters of 10/130 Tm:SIF (Nufern) while the signal input was splice to a fiber-coupled isolator (Thorlabs) that ensured

polarized output. To prevent parasitic lasing from Fresnel reflections, the Tm:SIF was angle cleaved at ~8°. This system could produce 25-30 mW of ASE before the onset of parasitic lasing.

Although the amplifier is designed for an all-fiber integration, the ASE source was not spliced directly to the pump combiner signal input. The fiber-coupled isolator contains a 7/125 fiber output while the pump combiner's signal input is 20/250. There was no MA at the time to join these dissimilar fibers, and optimizing and performing a taper was determined to be of no benefit for such initial characterizations. The ASE output was coupled into the pump combiner input using a 4.5 mm to 11 mm focal length lens system to optimally match the MFA and NA of the pump combiner's SIF input. A half-wave plate was used to align polarization to the stress rods, providing optimal coupling efficiencies and polarized output from the amplifier. Figure 20 shows the set-up used in testing amplification of the ASE source.

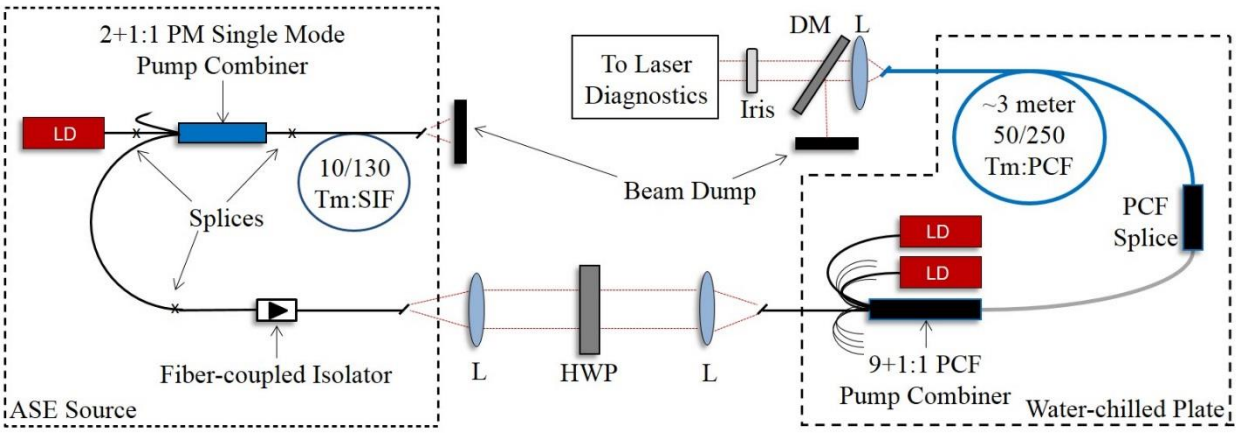

Figure 20. Set-up for characterizing amplification of a broadband ASE source. LD – 35 W, 79x nm pump diode, L – lens, HWP – half-wave plate, DM – dichroic mirror.

The amplifier was fastened to an aluminum plate water-cooled to 14 °C. Two 35 W, 79x nm (DILAS) pump diodes were spliced to the amplifier enabling ~70 W of usable pump power. At the

output, a dichroic mirror rejected unabsorbed 79x nm pump light and transmitted amplified 2 μm signal light, which was collimated and characterized.

Figure 21a shows the optical spectrum of the ASE source, while Figure 21b-f show the spectrum amplified at increasing pump powers. Figure 21f shows the onset of parasitic lasing, which occurred at pump powers of ~35 W.

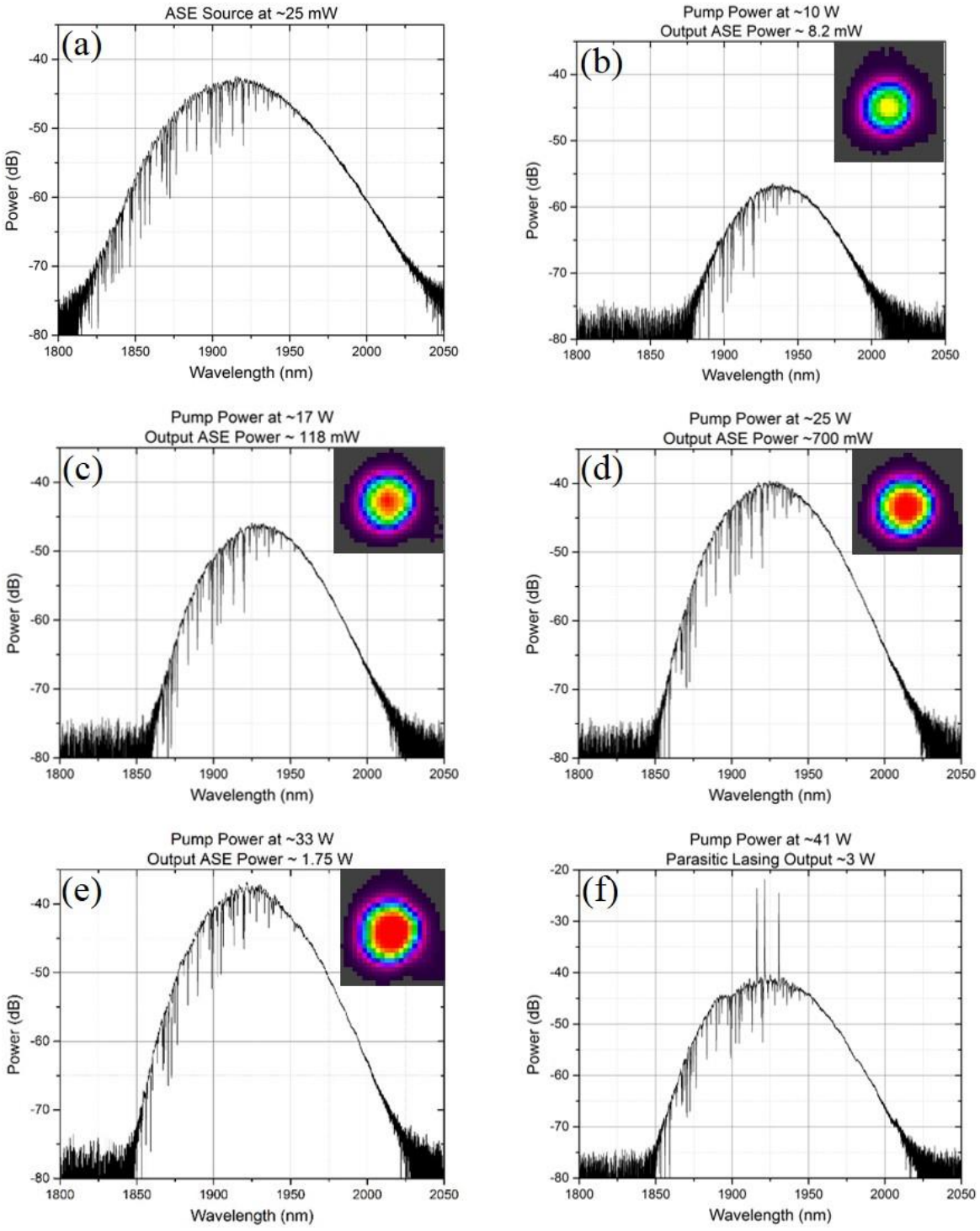

Figure 21. (a) Spectrum of the ASE source. (b-d) Amplified spectrum at pump powers of 10 W, 17 W, 25 W, 33 W. (f) Onset of parasitic lasing, which occurred at pump powers of ~35 W. Insets for (b-d) show the corresponding far-field beam images.

As seen in Figure 21a, the ASE source has spectral bandwidth > 100 nm at the -10 dB level, centered at 1915 nm. At 10 W of pump power, the spectral bandwidth is reduced due to reabsorption in the Tm:PCF. This occurs because of the quasi-three-level nature of Tm:fiber, in which shorter wavelengths are reabsorbed more strongly. In Figure 21c-e, reabsorption effects decrease as pump power is increased, resulting in a spectral bandwidth of ~90 nm at the -10 dB level for 33 W pump power, centered at ~1920 nm. The ASE source was amplified to a maximum of ~2 W output power before parasitic lasing occurred at pump powers of ~35 W, as seen in Figure 21f. The insets show the far-field beam profile, demonstrating Gaussian beam profile. Overall, this gain bandwidth of the Tm:PCF amplifier is capable of supporting sub-100 fs transform-limited pulses.

These amplified broadband spectra are also useful in characterizing the single-mode quality of the amplifier by looking for spectral modulations. If the amplifier was supporting HOM, the different propagation constants between the HOM and fundamental mode would produce periodic peaks and valleys in the amplified broadband spectrum, as seen in Figure 15. Throughout amplification, no spectral modulations were observed in the Tm:PCF amplifier, and manually perturbing the fiber had no observable effect on beam quality or spectrum. Based on this assessment, along with measurements detailed later, it is concluded that HOM are negligible.

A technique known as S^2 that utilizes spectral MMI fringes to detect HOM powers as low as 0.1 %, and was used to characterize passive 25/400 LMA SIF and 50/250 PCF [28]. The Tm-doped version of these fibers are used in the 3 MW system, and this integrated pump combiner, respectively. As seen in Figure 22, bend losses reduce HOM content in the LMA SIF, however ~5

% content remains in LP_{11} and LP_{02} modes. However, the PCF contains < 1 % HOM content in the LP_{11}, thus enabling virtually single-mode propagation. HOM content in the LMA SIF agrees with the MMI seen in the 3 MW system from Figure 15. The lack of HOM content in PCF supports the absence of spectral modulations in the amplified ASE spectra. This supports the conclusion that HOM are negligible in the integrated Tm:PCF amplifier.

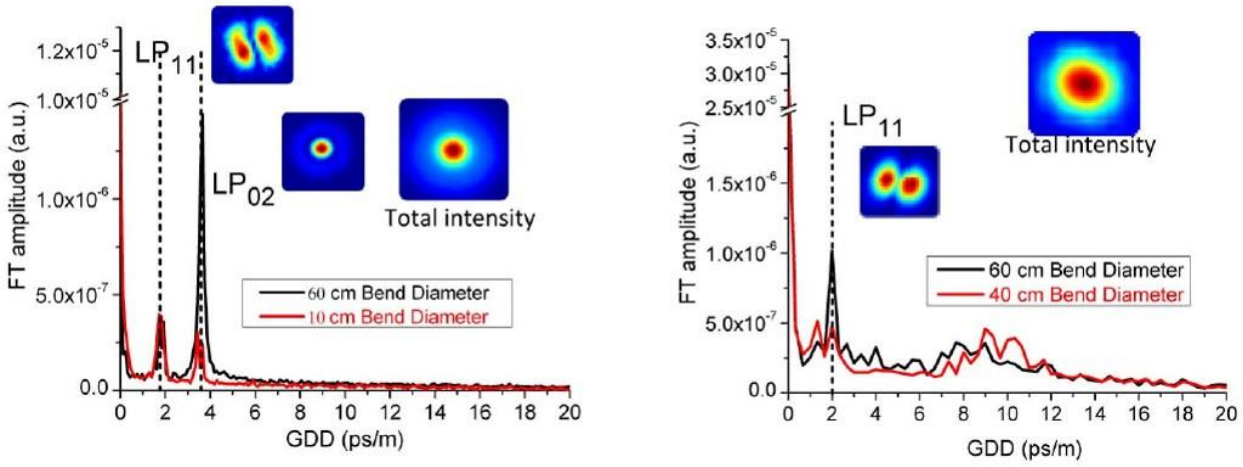

Figure 22. S^2 analysis to detect HOM content in (left) 25/400 LMA SIF and (right) 50/250 PCF [28].

Thus far, amplifying a broadband ASE source has demonstrated a large gain bandwidth and absence of MMI in the integrated amplifier. These traits are useful for amplification of USP while maintaining single-mode propagation. Next, the ASE source is modified to produce a laser seed to study the amplifier performance at higher power including beam quality, gain, and polarization maintaining properties.

5.3.2 Characterization using Laser Seed

An oscillator was constructed to investigate the amplification properties of the integrated pump combiner. This was accomplished by incorporating a feedback portion in the aforementioned ASE system, using a highly-reflective mirror at 2 μm. The fiber-coupled isolator was removed, and the output fiber was flat cleaved to form an output coupler from the ~4 % Fresnel reflection. This system produced ~680 mW output power operating at ~1985 nm. The laser seed was coupled through a free-space isolator into the pump combiner's signal input, as shown in Figure 23.

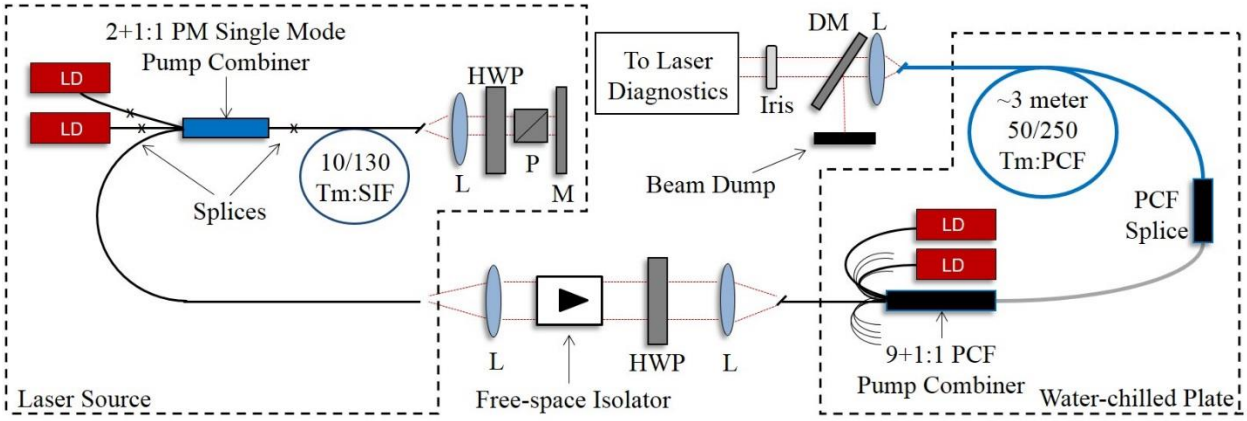

Figure 23. Set-up for characterizing amplification of a laser source. LD – 35 W, 79x nm pump diode, L – lens, HWP – half-wave plate, DM – dichroic mirror, P – polarizing beam cube, M – highly-reflective mirror at 2 μm.

First, a beam propagation factor, known as M^2, measurement was taken at ~10 W of pump power. M^2 is a quantitative tool to describe the focusing properties of a beam, in which the beam can be considered M^2-times diffraction-limited [136]. An $M^2 \cong 1$ implies the same focusing conditions as a diffraction-limited Gaussian beam. This is a common method used in characterizing laser systems to quantify beam quality. This was conducted by focusing the collimated output through a 500 mm lens, and measuring the beam width using a laser beam analysis software (Spiricon

Pyrocam III). Beam widths at several locations through the focus are acquired and fit to Equation 10, in which $w(z)$ are the measured beam widths along $\hat{z}$ (optic axis), w_0 is the minimum beam width, and z_0 is the location of w_0. Figure 24 shows the fitted data, demonstrating $M^2 < 1.1$ along both $\hat{x}$ and $\hat{y}$ axes.

$$w^2(z) = w_0^2 + M^4 \left(\frac{\lambda}{\pi w_0}\right)^2 (z - z_0)^2 \qquad (10)$$

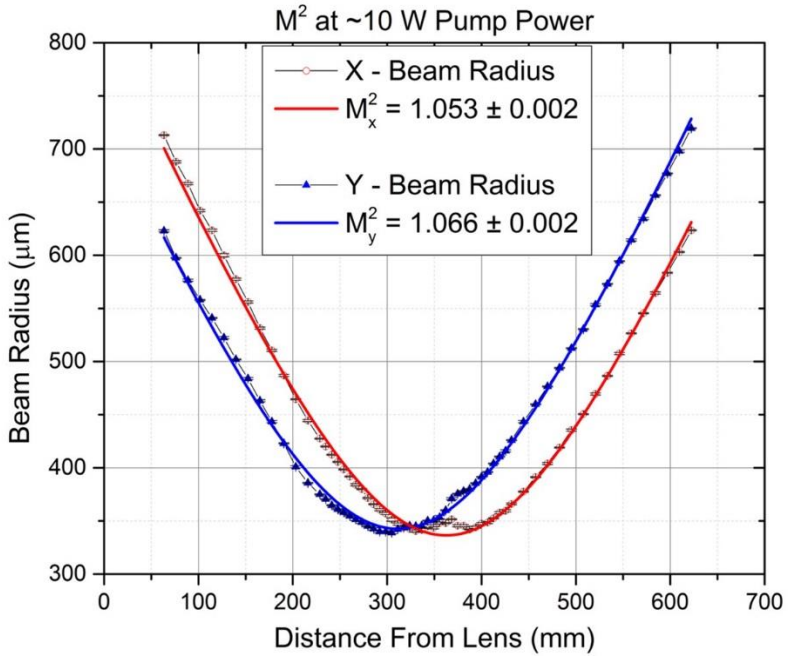

Figure 24. M^2 measurement taken at ~10 W of pump power for the amplified laser seed.

While the M^2 measurement is not a robust method to prove single-transverse mode beam quality, this result substantiates the conclusion that HOM content is negligible. Absence of spectral modulations in the amplified ASE spectra, $M^2 \cong 1$, and prior S^2-analysis revealing < 1 % HOM content in the passive PCF version all lead to a valid conclusion that HOM content is trivial and single-mode propagation is demonstrated in this integrated amplifier.

Next, the amplifier is operated at high pump powers to characterize the optical-to-optical slope efficiency. Because thulium operates at a high quantum defect as described in section 2.4, the Tm:PCF was held in a straight, 1-meter long V-groove to promote efficient heat extraction for investigating optimal efficiencies. As shown in Figure 22, the absence of bend losses allows ~5 % HOM content in the LP_{11} mode. This resulted in slight beam quality degradation that was observed at the output. Future iterations will incorporate a 40 cm diameter mandrel to allow sufficient bend losses and water-cooling operation.

Figure 25 shows the measured output power in the core by using an iris to filter out cladding light, as well as far-field beam profiles. Cladding light was measured to be 100 – 230 mW of total output power throughout amplification, and is therefore regarded as insignificant. ASE output power is also plotted for comparison, using an iris to filter cladding light as well. Absorbed pump power was calculated by multiplying by a factor of 0.92, and then subtracting unabsorbed pump power measured after the dichroic mirror at the output. This 0.92 factor was chosen because 92 % pump coupling was specified in a similar combiner discussed in [134]. The specifications in Table 1 show > 95 % pump coupling, however this was at 980 nm, not the 79x nm used here. Overall, these factors may provide a slightly lower estimate on true absorbed pump power.

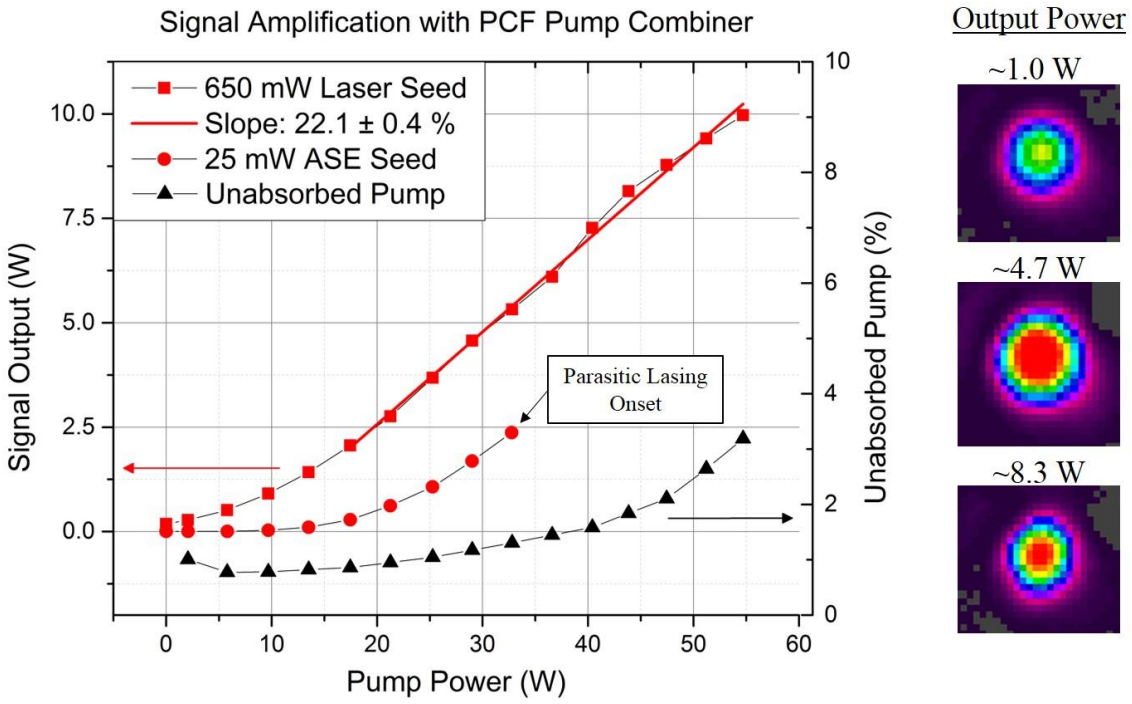

Figure 25. Left: Slope efficiencies (core light only) and unabsorbed pump power for the amplified seed. Right: Far-field beam profiles at denoted output powers.

A maximum output power of ~10 W was obtained at absorbed pump powers of ~55 W, demonstrating a 22.1 % slope efficiency. Unabsorbed pump power remained below 4 % throughout amplification. No roll-off in slope or saturation in pump absorption was observed. The beam exhibits a Gaussian profile despite the potential HOM content from keeping the PCF straight. The pump combiner is capable of supporting 9 pump diodes, correlating to ~300 W pump power. However, as discussed below, it is concluded the component is not fully optimized so it is premature to comment on the power scalability.

The signal throughput (zero pump power) including coupling losses and reabsorption was ~43 %, with ~64 % of that in the core. An identical pump combiner was used in [137] and appeared to

have 40-50 % signal throughput with spliced fiber coupling. These are much lower than the 67 % coupling specified, but a rigorous analysis is complicated because of reabsorption in the Tm:PCF. Nonetheless, the slope efficiency was low at 22.1 %. The identical pump combiner in [137] achieved only ~12 % slope efficiencies, however that system was operating at low seed powers of 100 – 120 mW with picosecond pulses at 50 kHz. For comparison, various seed powers were launched to investigate the effect on efficiency, seen in Figure 26. From this, higher efficiencies than ~12 % for coupled seed powers of 100 – 120 mW are expected.

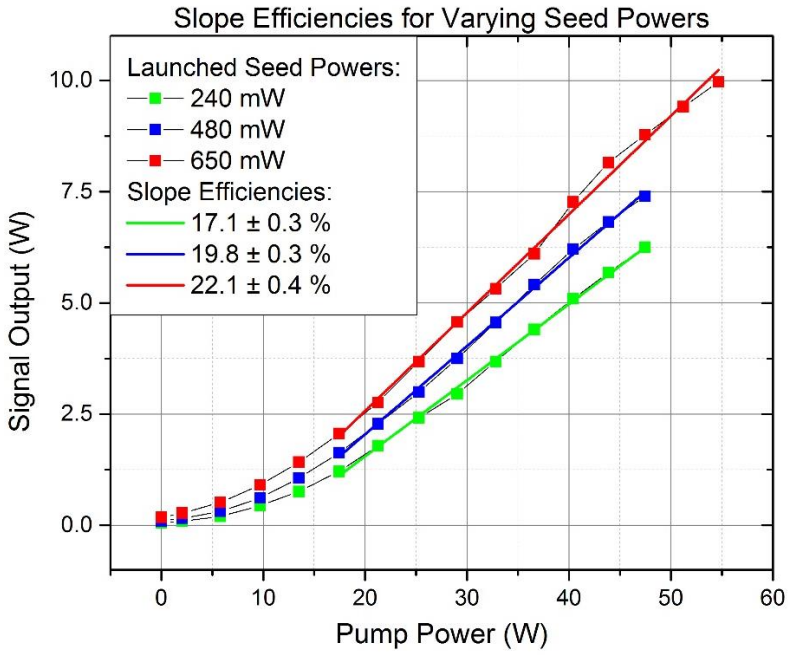

Figure 26. Slope efficiencies for varying seed powers.

Free-space coupling with counter-propagating pumping for Tm:PCF has demonstrated 36.6 % efficiencies for lasing [49], and 31.8 % efficiencies for amplification of nanosecond-pulses at 20 kHz [28]. The only CW amplification efficiencies reported for a similar Tm:PCF was 27.6 % [138]. In summary, amplification efficiencies > 30 % should be feasible for a Tm:PCF amplifier.

The low efficiency performance can be attributed to either: poor pump coupling, poor signal coupling, sub-optimal fiber length, or decreased performance by operating in co-propagating pump geometry. Poor pump coupling would lead to heat deposition in the pump combiner. To investigate this, an InSb thermal camera (FLIR SC7650) was used to image the combiner during amplification. Figure 27 shows a thermal image taken at the maximum pump power of ~55 W, with the annotated temperatures relative to temperatures with no pump.

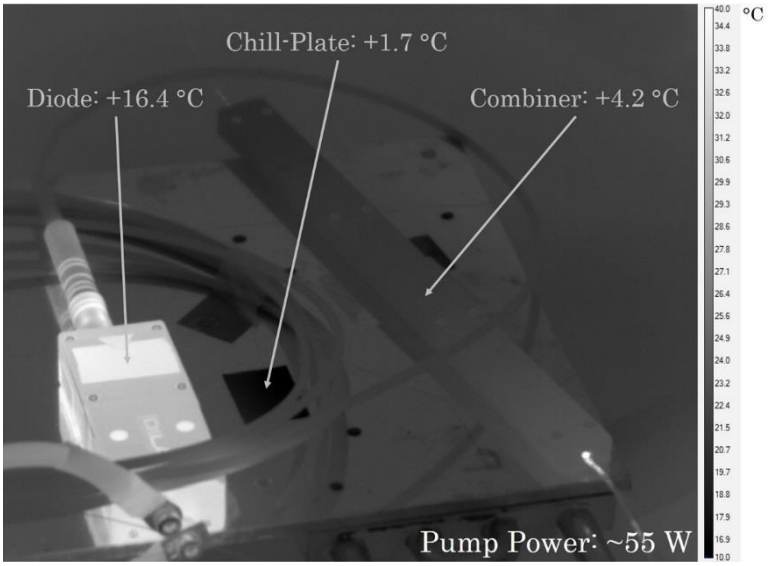

Figure 27. Thermal image of pump diode, water-chilled plate, and pump combiner at maximum pump power of ~55 W. Printed temperatures are relative to temperatures with no pump.

As seen in Figure 27, the water-chilled plate saw a minimal rise in temperature as expected. The pump diode temperature was elevated, as expected due to ~50 watts of heat generated per pump diode. The pump combiner saw a slight rise in temperature, but nothing indicative of detrimental scattered pump light from poor coupling. Also, no thermally conductive adhesive was used to optimally join the combiner to the water-chilled plate. Thus, these temperature increases could be

further reduced. Overall, pump coupling appears to be satisfactory, and not the cause for low efficiencies.

The three remaining possibilities are poor signal coupling, sub-optimal fiber length, or decreased performance by operating in co-propagating pump geometry. Unfortunately, proper characterization of the first two aspects would require deconstruction of the integrated amplifier, whereas counter-propagating amplification would damage the combiner. Further discussion and a potential outlook in regards to these concerns will be addressed in section 5.4 and Chapter 6.

Lastly, the polarization maintaining properties of the integrated amplifier were investigated. This was achieved by using a half-wave plate to rotate the polarization on a Glan-Taylor polarizing beam-splitter cube, then measuring maximum and minimum transmitted powers. This can be converted to a PER in decibels, as seen in Equation 4. The seed laser after the isolator was measured to have a PER of 29.5 ± 0.9 dB, primarily limited by the beam-splitting quality of the beam-splitter cube. The amplified output was characterized, and the PER can be seen in Figure 28.

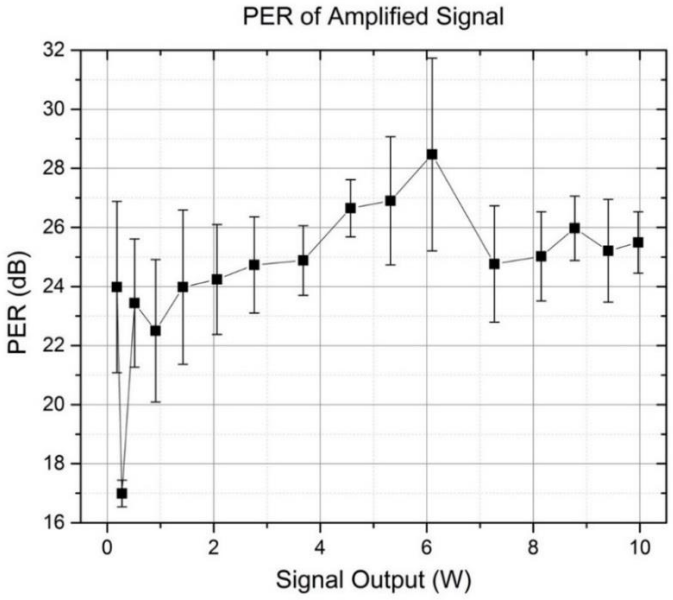

Figure 28. PER of the amplified seed throughout the amplification range.

The amplified output maintained a PER of ~25 dB up to the maximum power of ~10 W. At 0.25 W, a change of 4 mW in minimum polarization throughput can reduce PER from 24 dB to 17 dB. This is the cause of the PER dip at 0.25 W, and these sub-10 mW power fluctuations also induce the 1-2 dB standard deviations. These power fluctuations in measured PER were due to minor polarization state fluctuations. These fluctuations were observed when imaging the minimum power transmission through the polarizer. These polarization instabilities are likely due to imperfections at the taper or passive-to-active PCF splice, causing minute powers to be launched into the orthogonal polarization. Furthermore, this is potentially correlated to the low slope efficiencies seen earlier, from improper coupling in the combiner. Even so, PER of ~25 dB is impressive and demonstrates potential in power scaling of highly polarized Tm:PCF systems.

5.4 Experimental Conclusions

As previously discussed, the primary obstacle to scaling peak power beyond 3 MW in our Tm:fiber CPA system was mode quality degradation in the large MFA amplifier leading to MMI. Tm:PCF offers large gain bandwidth and very large MFA with nearly single-mode, diffraction-limited beam quality. However, the microstructured air hole design makes these fibers difficult to integrate into an all-fiber component. In this chapter, a novel all-fiber pump combiner that includes a Tm:PCF amplifier was described and characterized to determine its potential for all-fiber, high peak power USP amplification.

The most important characteristic investigated was the transverse mode quality of the amplifier. MMI severely degraded compressed pulse quality in LMA Tm:SIF as seen in Figure 15, and robust single-mode guidance is crucial to maintain transform-limited spectra. No spectral modulations were observed throughout amplification of a broadband ASE source in the integrated Tm:PCF amplifier, indicating negligible HOM content. An M^2 measurement was performed on an amplified seed laser, demonstrating $M^2 < 1.1$. Free-space coupled and free-space pumped systems have demonstrated excellent beam quality as well. This has been demonstrated in published S^2-analysis that measured < 0.1 % HOM content in passive PCF [28], indicating essentially single-mode quality. The integrated combiner maintained similar mode quality performance, and proves that the integrated combiner provides a pathway towards all-fiber, single-mode Tm:PCF amplification.

Additionally, the component demonstrated a high degree of polarization (PER ~ 25 dB), essentially single-mode propagation ($M^2 < 1.1$), and large gain bandwidth (~90 nm at -10 dB); however, the slope efficiency was sub-optimal at 22.1 %. Slope efficiencies greater than 30 % have been

reported in Tm:PCF with free-space signal and pump coupling [28, 49, 138]. So there is clearly room for pump combiner improvement in terms of efficiency. Low slope efficiencies must be attributed to poor pump coupling, poor signal coupling, sub-optimal fiber length, or decreased performance by operating in co-propagating pump geometry. Poor pump coupling was ruled out by lack of thermal signatures in the combiner at high pump powers.

In order to directly measure signal (and pump) coupling requires breaking the passive-to-active PCF splice; however until recently it would not be possible to re-splice the fibers. A recently-acquired CO_2-laser splicer facility is now in place but optimization of the PCF to PCF splicing is not yet complete. This is currently being addressed, and this capability will be available in the near future.

Performing a cut-back method, by removing portions of Tm:PCF, would enable analysis of the fiber length. This method is also used to measure pump/signal absorption by measuring pump/signal throughput as function of fiber length. However, this method inherently destroys the costly Tm:PCF. Breaking the passive-to-active splice would be more valuable than a cut-back method, as it allows reassembly of the amplifier.

Lastly, operating the pump combiner in a counter-propagating pump scheme to determine its effect on slope efficiency is not feasible. This would cause > 10 W of amplified seed being guided through the taper and out the SIF port, which goes against the manufactured design. This would damage the combiner, and possibly the pump diodes as well.

As a final comment, Figure 26 shows that the slope efficiency increases with higher seed powers. However, it is unlikely this increase would produce > 30 % slope efficiencies. The 10/130 preamplifier in the 3 MW system seeds the LMA Tm:SIF final amplifier with 50 – 100 mW. Thus, the 650 mW seed used in this characterization is a proof of concept high limit. If implemented into the 3 MW system, even lower slope efficiencies would result from the decreased seed power. It is important to note that the seed powers coupling into the Tm:PCF are unknown. Therefore, it is possible that the taper exhibits high signal loss and that insufficient seed power is the primary cause of the low efficiencies.

In general, a major theme of this thesis work is developing a protocol and test-bed for thoroughly characterizing thulium-doped amplifiers with the ultimate goal of improving the performance of USP amplification. This characterization is part of experiments to compare amplifiers based on Tm:SIF and Tm:PCF in free-space coupled, all-fiber, co-propagating pump, counter-propagating pump geometries in CW and pulsed operation. These levels of in-depth comparisons are important for future fiber amplifier design and implementation. Currently, the performance of the all-fiber PCF amplifier is being compared to a pre-existing free-space pump/signal coupled Tm:PCF amplifier as well as an all-fiber Tm:SIF LMA amplifier for high energy nanosecond pulse amplification

Ultimately, breaking the integrated amplifier's passive-to-active splice will allow accurate pump/signal coupling efficiencies to be measured without reabsorption effects. Also, the PER will be examined to determine if the polarization instabilities originated from the splice. Further characterization of the PCF pump combiner and the performance of Tm:PCF in as free-space

coupled amplifier will provide insight as to how to improve the all-fiber Tm:PCF amplifier, in particular to achieve slope efficiencies greater than 22.1 %. The ability to re-splice the Tm:PCF to the passive PCF will be critical to improving device performance.

These analyses provide an understanding of the various compromises necessary to achieve the best performance for 2 μm amplifiers. For example, to date Tm:SIF have demonstrated much higher average power and higher efficiency relative to Tm:PCF at the expense of mode quality and peak power scalability. As such, Tm:PCF has clear advantages for USP amplification whereas Tm:SIF LMA is better suited for high average power nanosecond pulse amplification.

Even without the benefits of cross-relaxation, the work described in this thesis indicate that this all-fiber Tm:PCF amplifier offers a path to scale peak power beyond the 3 MW level of our previous demonstrate. This work highlights further development and improvement necessary to achieve the promise of Tm:fiber to support USP systems with peak powers of ~100 kW in the fiber, with compressed peak powers of ~1 GW.

CHAPTER 6: CONCLUSIONS

In conclusion, scaling peak powers in USP fiber laser systems was discussed. As described in Chapter 3, generating high peak powers in fiber waveguides is limited by the onset of NLE, such as self-focusing, SPM, SRS, and SBS. These NLE are driven by high optical intensities. Two ways to mitigate high intensities inside the fiber are scaling pulse duration or scaling MFA. Scaling pulse duration is routinely accomplished using CPA. Scaling MFA in SIF was shown in Chapter 2 to be limited to ~400 μm^2 because further increase caused unwanted HOM to propagate. HOM content in the custom-built, 3 MW system produced MMI which degraded the compressed pulse spectrum and limited further peak power scaling. To combat this, PCF architecture enables both large MFA of ~1000 μm^2 and nearly single-mode guidance. With all of these factors taken into account, it is imperative to further investigate PCF-based amplifiers in terms of peak power scaling.

While PCF is attractive, the microstructured design and air holes make PCF difficult to integrate into all-fiber components. "All-fiber" laser systems, as discussed in Chapter 4, are valuable for their environmental stability and compact footprint. Recent developments have seen pump combiners incorporating PCF geometry that are capable of handling kW-level pump powers. This thesis describes the performance of the first of its kind, all-fiber pump combiner spliced to a thulium-doped PCF, enabling an all-fiber PCF amplifier at 2 μm. This innovative component is the primary focus for experimental characterization, as detailed in Chapter 5.

Thulium-doped fibers are used in this research because they offer a large gain bandwidth, reduced NLE, and applications at 2 μm. The large gain bandwidth is crucial for amplifying sub-100

femtosecond pulses without gain narrowing. The 2 μm output wavelength inherently suppresses NLE such as self-focusing, SPM, and SRS as compared to 1 μm. Also, this output wavelength makes it attractive for supporting applications towards the mid-IR, such as supercontinuum generation.

An integrated pump combiner and Tm:PCF amplifier was characterized using a CW source to determine its feasibility in increasing USP peak powers. A crucial attribute for this component is the demonstration of single-mode propagation. A broadband ASE source was amplified by the Tm:PCF combiner to observe the gain bandwidth as well as look for spectral modulations. The gain bandwidth was > 90 nm at the -10 dB level, indicating the ability to amplify sub-100 femtosecond pulses.

No spectral modulations were observed with amplification, a positive sign that HOM content is minimal. The ASE seed was converted to a laser, and beam quality measurements show $M^2 < 1.1$. These results, along with a previously published S^2 analysis showing < 1 % HOM content in passive PCF, confirms that the integrated Tm:PCF amplifier operates with essentially single-mode beam quality. This is a vital assessment showing that PCF will mitigate MMI as compared to the LMA Tm:SIF used in the 3 MW system.

The 650 mW laser source was used to seed the amplifier, generating 10 W of output power and 22.1 % slope efficiency, as well as a PER of ~25 dB. Free-space systems utilizing similar Tm:PCF have seen upwards of 30 % or greater efficiencies. The low efficiencies seen with the integrated amplifier could be attributed to: poor pump coupling, poor signal coupling, sub-optimal fiber length, or differences arising from co-propagating versus counter-propagating pump schemes.

Thermal images of the combiner show minimal heating at the highest pump powers, concluding that pump coupling is likely sufficient. Increasing the launched seed power does increase the slope; however, the extent is the subject of further investigation. Nonetheless, the amount of coupled seed power into the Tm:PCF is unknown. The free-space systems with greater than 30 % efficiency all used counter-propagating pump schemes to promote higher gain. Operating the pump combiner in this configuration would certainly cause damage. Thus, an accurate comparison between the integrated and free-space amplifier requires a more thorough investigation of the free-space amplifier performance in co-propagating configurations.

Overall, the all-fiber pump combiner and Tm:PCF amplifier demonstrated a large gain bandwidth, single-mode propagation, and high degree of polarization. These attributes, notably the single-mode propagation, make it attractive for further peak power scaling at 2 μm. Optimizing a splice routine for PCF will allow the passive-to-active splice to be broken knowing it can be replaced. By doing this, an accurate analysis of signal and pump coupling can be examined. Determining the source of low efficiency will allow customer feedback and an optimized version to be developed. Constructing a co-propagating free-space Tm:PCF amplifier will enable direct comparison with the integrated amplifier. Also, an additional USP source that operates within the gain bandwidth of Tm:PCF will be developed to allow incorporation of the integrated Tm:PCF amplifier. Between these three future goals, a detailed understanding of Tm:PCF amplifiers will be gained, as well as direct comparisons of parameters such as: co- versus counter-propagating pump schemes, Tm:SIF versus Tm:PCF performances, free-space versus all-fiber configurations, and CW versus USP characteristics. Moving towards an all-fiber PCF amplifier is imperative to continue further progress towards ~1 GW USP peak powers at 2 μm.

REFERENCES

1. T. Brabec and F. Krausz, "Intense few-cycle laser fields: Frontiers of nonlinear optics," Reviews of Modern Physics **72**, 545-591 (2000).

2. S. H. Chung and E. Mazur, "Surgical applications of femtosecond lasers," Journal of Biophotonics **2**, 557-572 (2009).

3. R. R. Gattass and E. Mazur, "Femtosecond laser micromachining in transparent materials," Nature Photonics **2**, 7 (2008).

4. H. G. Roskos, M. D. Thomson, M. Kreß, and T. Löffler, "Broadband THz emission from gas plasmas induced by femtosecond optical pulses: From fundamentals to applications," Laser & Photonics Reviews **1**, 349-368 (2007).

5. M. D. Shirk and P. A. Molian, "A review of ultrashort pulsed laser ablation of materials," Journal of Laser Applications **10**, 18-28 (1998).

6. W. Sibbett, A. A. Lagatsky, and C. T. A. Brown, "The development and application of femtosecond laser systems," Opt. Express **20**, 6989-7001 (2012).

7. H. L. Xu and S. L. Chin, "Femtosecond Laser Filamentation for Atmospheric Sensing," Sensors **11**, 32-53 (2010).

8. R. Andrew Sims, P. Kadwani, L. Shah, A. Sincore, and M. Richardson, "1 μJ, sub-500 fs chirped pulse amplification in a Tm-doped fiber system," Opt. Lett. **38**, 121-123 (2013).

9. S. E. A. Bahaa and M. C. Teich, *Fundamentals of Photonics,* 2 ed., Pure and Applied Optics (Wiley, 2007).

10. T. Li, *Optical Fiber Communications: Fiber Fabrication* (Elsevier, 1985).

11. P. L. LiKamWa, "Guided Waves and Optoelectronics," (CREOL, The College of Optics and Photonics, Spring 2013).

12. A. W. Snyder and J. Love, *Optical Waveguide Theory* (Springer, 1983).

13. R. Paschotta, "Encyclopedia of Laser Physics and Technology", retrieved 2013, http://www.rp-photonics.com/lp_modes.html.

14. R. Billington, "Effective Area of Optical Fibres Definition and Measurement Techniques," (Centre for Optical and Environmental Metrology, National Physical Laboratory, 1999).

15. M. R. Vastag, "Mode Field Diameter and Effective Area: White Paper," (Corning, 2001).

16. J. Noda, K. Okamoto, and Y. Sasaki, "Polarization-maintaining fibers and their applications," Lightwave Technology, Journal of **4**, 1071-1089 (1986).

17. T. Hosaka, K. Okamoto, T. Miya, Y. Sasaki, and T. Edahiro, "Low-loss single polarisation fibres with asymmetrical strain birefringence," Electronics Letters **17**, 530-531 (1981).

18. A. Liem, J. Limpert, T. Schreiber, M. Reich, H. Zellmer, A. Tünnermann, A. Carter, and K. Tankala, "High power linearly polarized fiber laser," in *Conference on Lasers and Electro-Optics/International Quantum Electronics Conference and Photonic Applications Systems Technologies*, Technical Digest (CD) (Optical Society of America, 2004), CMS4.

19. L. Shah, R. A. Sims, P. Kadwani, C. C. C. Willis, J. B. Bradford, A. Pung, M. K. Poutous, E. G. Johnson, and M. Richardson, "Integrated Tm:fiber MOPA with polarized output and narrow linewidth with 100 W average power," Opt. Express **20**, 20558-20563 (2012).

20. D. A. Nolan, G. E. Berkey, M.-J. Li, X. Chen, W. A. Wood, and L. A. Zenteno, "Single-polarization fiber with a high extinction ratio," Opt. Lett. **29**, 1855-1857 (2004).

21. E. Snitzer, H. Po, F. Hakimi, R. Tumminelli, and B. C. McCollum, "Double Clad, Offset Core Nd Fiber Laser," in *Optical Fiber Sensors*, OSA Technical Digest Series (Optical Society of America, 1988), PD5.

22. V. Dominic, S. MacCormack, R. Waarts, S. Sanders, S. Bicknese, R. Dohle, E. Wolak, P. S. Yeh, and E. Zucker, "110 W fiber laser," in *CLEO, Conference on Lasers and Electro-Optics*, 1999), CPD11-11.

23. D. J. Richardson, J. Nilsson, and W. A. Clarkson, "High power fiber lasers: current status and future perspectives [Invited]," J. Opt. Soc. Am. B **27**, B63-B92 (2010).

24. D. Marcuse, "Curvature loss formula for optical fibers," J. Opt. Soc. Am. **66**, 216-220 (1976).

25. D. Marcuse, "Influence of curvature on the losses of doubly clad fibers," Appl. Opt. **21**, 4208-4213 (1982).

26. J. P. Koplow, D. A. V. Kliner, and L. Goldberg, "Single-mode operation of a coiled multimode fiber amplifier," Opt. Lett. **25**, 442-444 (2000).

27. C. Schulze, A. Lorenz, D. Flamm, A. Hartung, S. Schröter, H. Bartelt, and M. Duparré, "Mode resolved bend loss in few-mode optical fibers," Opt. Express **21**, 3170-3181 (2013).

28. P. Kadwani, C. Jollivet, R. A. Sims, A. Schülzgen, L. Shah, and M. Richardson, "Comparison of higher-order mode suppression and Q-switched laser performance in thulium-doped large mode area and photonic crystal fibers," Opt. Express **20**, 24295-24303 (2012).

29. M.-J. Li, X. Chen, A. Liu, S. Gray, J. Wang, D. T. Walton, and L. A. Zenteno, "Limit of Effective Area for Single-Mode Operation in Step-Index Large Mode Area Laser Fibers," J. Lightwave Technol. **27**, 3010-3016 (2009).

30. A. E. Siegman, "Gain-guided, index-antiguided fiber lasers," J. Opt. Soc. Am. B **24**, 1677-1682 (2007).

31. A. E. Siegman, Y. Chen, V. Sudesh, M. Richardson, M. Bass, P. Foy, W. Hawkins, and J. Ballato, "Confined propagation and near single-mode laser oscillation in a gain-guided, index antiguided optical fiber," Applied Physics Letters **89**, 251101 (2006).

32. P. Wang, L. J. Cooper, J. K. Sahu, and W. A. Clarkson, "Efficient single-mode operation of a cladding-pumped ytterbium-doped helical-core fiber laser," Opt. Lett. **31**, 226-228 (2006).

33. J. R. Marciante, "Gain Filtering for Single-Spatial-Mode Operation of Large-Mode-Area Fiber Amplifiers," IEEE J. Sel. Top. Quant. Electron. **15**, 30-36 (2009).

34. C.-H. Liu, G. Chang, N. Litchinister, D. Guertin, N. Jacobson, K. Tankala, and A. Galvanauskas, "Chirally Coupled Core Fibers at 1550-nm and 1064-nm for Effectively Single-Mode Core Size Scaling," in *Conference on Lasers and Electro-Optics/Quantum Electronics and Laser Science Conference and Photonic Applications Systems Technologies*, OSA Technical Digest Series (CD) (Optical Society of America, 2007), CTuBB3.

35. X. Peng, K. Kim, M. Mielke, T. Booth, J. W. Nicholson, J. M. Fini, X. Liu, A. DeSantolo, P. S. Westbrook, R. S. Windeler, E. M. Monberg, F. V. DiMarcello, C. Headley, and D. J. DiGiovanni, "Higher-order mode fiber enables high energy chirped-pulse amplification," Opt. Express **21**, 32411-32416 (2013).

36. M. E. Fermann, "Single-mode excitation of multimode fibers with ultrashort pulses," Opt. Lett. **23**, 52-54 (1998).

37. J. C. Knight, T. A. Birks, P. S. J. Russell, and D. M. Atkin, "All-silica single-mode optical fiber with photonic crystal cladding," Opt. Lett. **21**, 1547-1549 (1996).

38. P. Russell, "Photonic Crystal Fibers," Science **299**, 358-362 (2003).

39. S. A. Cerqueira Jr, "Recent progress and novel applications of photonic crystal fibers," Rep. Prog. Phys. **73**, 024401 (2010).

40. J. M. Dudley, G. Genty, and S. Coen, "Supercontinuum generation in photonic crystal fiber," Reviews of Modern Physics **78**, 1135-1184 (2006).

41. J. C. Knight, "Photonic crystal fibers and fiber lasers (Invited)," J. Opt. Soc. Am. B **24**, 1661-1668 (2007).

42. A. M. R. Pinto and M. Lopez-Amo, "Photonic Crystal Fibers for Sensing Applications," Journal of Sensors **2012**, 21 (2012).

43. J. Limpert, F. Stutzki, F. Jansen, H.-J. Otto, T. Eidam, C. Jauregui, and A. Tunnermann, "Yb-doped large-pitch fibres: effective single-mode operation based on higher-order mode delocalisation," Light Sci Appl **1**, e8 (2012).

44. J. C. Knight, T. A. Birks, P. S. J. Russell, and J. P. de Sandro, "Properties of photonic crystal fiber and the effective index model," J. Opt. Soc. Am. A **15**, 748-752 (1998).

45. X.-F. Bao, X.-J. Wang, H. Su, and X.-J. Shu, "Geometric definition of the V-parameter in photonic crystal fibers," Opt. Lett. **39**, 892-895 (2014).

46. N. A. Mortensen, J. R. Folkenberg, M. D. Nielsen, and K. P. Hansen, "Modal cutoff and the V parameter in photonic crystal fibers," Opt. Lett. **28**, 1879-1881 (2003).

47. T. A. Birks, J. C. Knight, and P. S. J. Russell, "Endlessly single-mode photonic crystal fiber," Opt. Lett. **22**, 961-963 (1997).

48. J. Limpert, A. Liem, M. Reich, T. Schreiber, S. Nolte, H. Zellmer, A. Tünnermann, J. Broeng, A. Petersson, and C. Jakobsen, "Low-nonlinearity single-transverse-mode ytterbium-doped photonic crystal fiber amplifier," Opt. Express **12**, 1313-1319 (2004).

49. N. Modsching, P. Kadwani, R. A. Sims, L. Leick, J. Broeng, L. Shah, and M. Richardson, "Lasing in thulium-doped polarizing photonic crystal fiber," Opt. Lett. **36**, 3873-3875 (2011).

50. F. Röser, T. Eidam, J. Rothhardt, O. Schmidt, D. N. Schimpf, J. Limpert, and A. Tünnermann, "Millijoule pulse energy high repetition rate femtosecond fiber chirped-pulse amplification system," Opt. Lett. **32**, 3495-3497 (2007).

51. C. D. Brooks and F. Di Teodoro, "Multimegawatt peak-power, single-transverse-mode operation of a 100μm core diameter, Yb-doped rodlike photonic crystal fiber amplifier," Applied Physics Letters **89**, 111119 (2006).

52. C. Gaida, P. Kadwani, L. Leick, J. Broeng, L. Shah, and M. Richardson, "CW-lasing and amplification in Tm3+-doped photonic crystal fiber rod," Opt. Lett. **37**, 4513-4515 (2012).

53. H. P. Uranus, "Theoretical study on the multimodeness of a commercial endlessly single-mode PCF," Optics Communications **283**, 4649-4654 (2010).

54. F. Jansen, F. Stutzki, H.-J. Otto, M. Baumgartl, C. Jauregui, J. Limpert, and A. Tünnermann, "The influence of index-depressions in core-pumped Yb-doped large pitch fibers," Opt. Express **18**, 26834-26842 (2010).

55. L. Dong, X. Peng, and J. Li, "Leakage channel optical fibers with large effective area," J. Opt. Soc. Am. B **24**, 1689-1697 (2007).

56. T. Eidam, J. Rothhardt, F. Stutzki, F. Jansen, S. Hädrich, H. Carstens, C. Jauregui, J. Limpert, and A. Tünnermann, "Fiber chirped-pulse amplification system emitting 3.8 GW peak power," Opt. Express **19**, 255-260 (2011).

57. F. Jansen, F. Stutzki, C. Jauregui, J. Limpert, and A. Tünnermann, "High-power very large mode-area thulium-doped fiber laser," Opt. Lett. **37**, 4546-4548 (2012).

58. C. Gaida, M. Gebhardt, P. Kadwani, L. Leick, J. Broeng, L. Shah, and M. Richardson, "Amplification of nanosecond pulses to megawatt peak power levels in Tm3+-doped photonic crystal fiber rod," Opt. Lett. **38**, 691-693 (2013).

59. F. Stutzki, F. Jansen, A. Liem, C. Jauregui, J. Limpert, and A. Tünnermann, "26 mJ, 130 W Q-switched fiber-laser system with near-diffraction-limited beam quality," Opt. Lett. **37**, 1073-1075 (2012).

60. F. Stutzki, F. Jansen, C. Jauregui, J. Limpert, and A. Tünnermann, "2.4 mJ, 33 W Q-switched Tm-doped fiber laser with near diffraction-limited beam quality," Opt. Lett. **38**, 97-99 (2013).

61. S. D. Agger and J. H. Povlsen, "Emission and absorption cross section of thulium doped silica fibers," Opt. Express **14**, 50-57 (2006).

62. D. A. Simpson, "Spectroscopy of thulium doped silica glass," (PhD Dissertation, Victoria University, 2008).

63. S. D. Jackson, "The spectroscopic and energy transfer characteristics of the rare earth ions used for silicate glass fibre lasers operating in the shortwave infrared," Laser & Photonics Reviews **3**, 466-482 (2009).

64. I. Photonics, "ELR Series: CW Erbium Fiber Lasers" (2014), retrieved http://www.ipgphotonics.com/Collateral/Documents/English-US/ELR%20datasheet_IPG.pdf.

65. D. Y. Shen, J. K. Sahu, and W. A. Clarkson, "High-power widely tunable Tm:fibre lasers pumped by an Er,Yb co-doped fibre laser at 1.6 μm," Opt. Express **14**, 6084-6090 (2006).

66. DILAS, "Fiber Coupled Single Bar Modules", retrieved http://www.dilas.com/pages/products.php?category=22&series=40.

67. S. D. Jackson, "Cross relaxation and energy transfer upconversion processes relevant to the functioning of 2 μm Tm3+-doped silica fibre lasers," Optics Communications **230**, 197-203 (2004).

68. S. D. Jackson and S. Mossman, "Efficiency Dependence on the Tm3+ and Al3+ Concentrations for Tm3+-Doped Silica Double-Clad Fiber Lasers," Appl. Opt. **42**, 2702-2707 (2003).

69. "Gemini Observatory: IR Transmission Spectra" (Lord, S. D. - NASA Technical Memorandum 103957, 1992), retrieved http://www.gemini.edu/sciops/telescopes-and-sites/observing-condition-constraints/ir-transmission-spectra.

70. T. S. McComb, R. A. Sims, C. C. C. Willis, P. Kadwani, V. Sudesh, L. Shah, and M. Richardson, "High-power widely tunable thulium fiber lasers," Appl. Opt. **49**, 6236-6242 (2010).

71. G. D. Spiers, R. T. Menzies, J. Jacob, L. E. Christensen, M. W. Phillips, Y. Choi, and E. V. Browell, "Atmospheric CO2 measurements with a 2 μm airborne laser absorption spectrometer employing coherent detection," Appl. Opt. **50**, 2098-2111 (2011).

72. V. Sudesh, T. McComb, R. Sims, L. Shah, and M. Richardson, "High Power, Tunable, CW, Narrow Line Thulium Fiber Laser for Ranging Applications," in *Advanced Solid-*

State Photonics, OSA Technical Digest Series (CD) (Optical Society of America, 2009), WB1.

73. N. M. Fried, "Thulium fiber laser lithotripsy: An in vitro analysis of stone fragmentation using a modulated 110-watt Thulium fiber laser at 1.94 μm," Lasers in Surgery and Medicine **37**, 53-58 (2005).

74. D. Creeden, M. Jiang, P. A. Budni, P. A. Ketteridge, S. D. Setzler, Y. E. Young, J. C. McCarthy, P. G. Schunemann, T. M. Pollak, P. Tayebati, and E. P. Chicklis, "Thulium fiber laser-pumped mid-IR OPO," in *Laser Source Technology for Defense and Security IV*, 2008), 69520S.

75. M. Gebhardt, C. Gaida, P. Kadwani, A. Sincore, N. Gehlich, C. Jeon, L. Shah, and M. Richardson, "High peak-power mid-infrared ZnGeP2 optical parametric oscillator pumped by a Tm:fiber master oscillator power amplifier system," Opt. Lett. **39**, 1212-1215 (2014).

76. J. Swiderski and M. Michalska, "Mid-infrared supercontinuum generation in a single-mode thulium-doped fiber amplifier," Laser Physics Letters **10**, 035105 (2013).

77. N. Granzow, M. A. Schmidt, W. Chang, L. Wang, Q. Coulombier, J. Troles, P. Toupin, I. Hartl, K. F. Lee, M. E. Fermann, L. Wondraczek, and P. S. J. Russell, "Mid-infrared supercontinuum generation in As2S3-silica "nano-spike" step-index waveguide," Opt. Express **21**, 10969-10977 (2013).

78. A. V. Smith and B. T. Do, "Bulk and surface laser damage of silica by picosecond and nanosecond pulses at 1064 nm," Appl. Opt. **47**, 4812-4832 (2008).

79. C. Jauregui, J. Limpert, and A. Tunnermann, "High-power fibre lasers," Nat Photon **7**, 861-867 (2013).

80. R. H. Stolen and A. Ashkin, "Optical Kerr effect in glass waveguide," Applied Physics Letters **22**, 294-296 (1973).

81. G. Fibich and A. L. Gaeta, "Critical power for self-focusing in bulk media and in hollow waveguides," Opt. Lett. **25**, 335-337 (2000).

82. K. S. Kim, W. A. Reed, K. W. Quoi, and R. H. Stolen, "Measurement of the nonlinear index of silica-core and dispersion-shifted fibers," Opt. Lett. **19**, 257-259 (1994).

83. A. Galvanauskas, C. Ming-Yuan, B. Hou, and K.-H. Liao, "High Peak Power Pulse Amplification in Large-Core Yb-Doped Fiber Amplifiers," Selected Topics in Quantum Electronics, IEEE Journal of **13**, 559-566 (2007).

84. G. Tempea and T. Brabec, "Theory of self-focusing in a hollow waveguide," Opt. Lett. **23**, 762-764 (1998).

85. R. H. Stolen and C. Lin, "Self-phase-modulation in silica optical fibers," Physical Review A **17**, 1448-1453 (1978).

86. G. P. Agrawal, *Nonlinear Fiber Optics*, 3 ed., Optics and Photonics (Academic Press, 2001).

87. R. H. Stolen and E. P. Ippen, "Raman gain in glass optical waveguides," Applied Physics Letters **22**, 276-278 (1973).

88. F. M. Mitschke and L. F. Mollenauer, "Discovery of the soliton self-frequency shift," Opt. Lett. **11**, 659-661 (1986).

89. R. A. Sims, P. Kadwani, H. Ebendorff-Heideprem, L. Shah, T. Monro, and M. Richardson, "Chirped pulse amplification in single mode Tm:fiber using a chirped Bragg grating," Applied Physics B **111**, 299-304 (2013).

90. J. W. Nicholson, A. D. Yablon, S. Ramachandran, and S. Ghalmi, "Spatially and spectrally resolved imaging of modal content in large-mode-area fibers," Opt. Express **16**, 7233-7243 (2008).

91. D. Strickland and G. Mourou, "Compression of amplified chirped optical pulses," Optics Communications **55**, 447-449 (1985).

92. J. Limpert, T. Clausnitzer, A. Liem, T. Schreiber, H. J. Fuchs, H. Zellmer, E. B. Kley, and A. Tnnermann, "High-average-power femtosecond fiber chirped-pulse amplification system," Opt. Lett. **28**, 1984-1986 (2003).

93. F. Röser, J. Rothhard, B. Ortac, A. Liem, O. Schmidt, T. Schreiber, J. Limpert, and A. Tünnermann, "131 W 220 fs fiber laser system," Opt. Lett. **30**, 2754-2756 (2005).

94. G. Imeshev and M. Fermann, "230-kW peak power femtosecond pulses from a high power tunable source based on amplification in Tm-doped fiber," Opt. Express **13**, 7424-7431 (2005).

95. F. Haxsen, D. Wandt, U. Morgner, J. Neumann, and D. Kracht, "Pulse energy of 151 nJ from ultrafast thulium-doped chirped-pulse fiber amplifier," Opt. Lett. **35**, 2991-2993 (2010).

96. P. Wan, L.-M. Yang, and J. Liu, "High pulse energy 2 μm femtosecond fiber laser," Opt. Express **21**, 1798-1803 (2013).

97. "Eye Safe 25P/250 Thulium-Doped LMA Double Clad Fiber" (Nufern, 2014), retrieved http://www.nufern.com/pam/optical_fibers/11/LMA-TDF-25P_250-HE/.

98. A. Klenke, S. Breitkopf, M. Kienel, T. Gottschall, T. Eidam, S. Hädrich, J. Rothhardt, J. Limpert, and A. Tünnermann, "530 W, 1.3 mJ, four-channel coherently combined femtosecond fiber chirped-pulse amplification system," Opt. Lett. **38**, 2283-2285 (2013).

99. M. Kienel, A. Klenke, T. Eidam, M. Baumgartl, C. Jauregui, J. Limpert, and A. Tünnermann, "Analysis of passively combined divided-pulse amplification as an energy-scaling concept," Opt. Express **21**, 29031-29042 (2013).

100. R. Kashyap, *Fiber Bragg Gratings* (Academic press, 1999).

101. L. Sun, S. Jiang, J. D. Zuegel, and J. R. Marciante, "All-fiber optical isolator based on Faraday rotation in highly terbium-doped fiber," Opt. Lett. **35**, 706-708 (2010).

102. E. H. Turner and R. H. Stolen, "Fiber Faraday circulator or isolator," Opt. Lett. **6**, 322-323 (1981).

103. "1 micron all-fiber isolator" (AdValue Photonics, Inc., 2014), retrieved http://www.advaluephotonics.com/images/media/SpecSheet/ap-aiso.pdf.

104. "IR Fiber Optic Isolators" (Thorlabs, 2014), retrieved http://www.thorlabs.com/newgrouppage9.cfm?objectgroup_id=6763.

105. "2 micron fiber isolator" (AdValue Photonics, Inc., 2014), retrieved http://www.advaluephotonics.com/images/media/SpecSheet/ap-iso-2000pi_and_2000pm.pdf.

106. "Optical components for fiber laser unit" (Shinkosha, 2014), retrieved http://www.shinkosha.com/english/sehin/4_02.html.

107. "Reflector for High-power Fiber Lasers" (TeraXion, 2014), retrieved http://www.teraxion.com/en/pws-hpr.

108. "Fiber laser mirror gratings" (ITF Labs, 2014), retrieved http://www.3spgroup.com/3SPG/ProductsCOM.php?locale=en&Line_no=14&sub_category_id=5211&cat_category_id=200.

109. "Visible and 2um Wavelength Fiber Grating" (O/E Land, Inc., 2014), retrieved http://www.o-eland.com/FiberGratingProducts/FiberGrating_visible_2um.htm.

110. M. Faucher and Y. K. Lize, "Mode field adaptation for high power fiber lasers," in *Conference on Lasers and Electro-Optics*, (Optical Society of America, 2007), CFI7.

111. "Industrial and Fiber Laser Components" (ITF Labs, 2014), retrieved http://www.3spgroup.com/ITFLabs/Applications_home.php?locale=en&Application_no=22.

112. F. Gonthier, L. Martineau, N. Azami, M. Faucher, F. Seguin, D. Stryckman, and A. Villeneuve, "High-power All-Fiber components: the missing link for high-power fiber lasers," in *Fiber Lasers: Technology, Systems, and Applications*, 2004), 266-276.

113. D. J. DiGiovanni and A. J. Stentz, "Tapered fiber bundles for coupling light into and out of cladding-pumped fiber devices," (U.S. Patent 5864644, 1999).

114. C. Headley Iii, M. Fishteyn, A. D. Yablon, M. J. Andrejco, K. Brar, J. Mann, M. D. Mermelstein, and D. J. DiGiovanni, "Tapered fiber bundles for combining laser pumps

(Invited Paper)," in *Fiber Lasers II: Technology, Systems, and Applications*, 2005), 263-272.

115. Q. Xiao, P. Yan, J. He, Y. Wang, X. Zhang, and M. Gong, "Tapered fused fiber bundle coupler capable of 1 kW laser combining and 300 W laser splitting," Laser Phys. **21**, 1415-1419 (2011).

116. A. Wetter, M. Faucher, M. Lovelady, and F. Séguin, "Tapered fused-bundle splitter capable of 1kW CW operation," in *Fiber Lasers IV: Technology, Systems, and Applications*, 2007), 64530I.

117. "Passive Multimode Components" (ITF Labs, 2014), retrieved http://www.itflabs.com/ITFLabs/Products.php?locale=en&Line_no=11&sub_category_id=5108&cat_category_id=110.

118. "High Power N+1:1 Coupler" (Nufern, 2014), retrieved http://www.nufern.com/filestorage/banners/pdf/file_51.pdf.

119. M. H. Muendel, R. Farrow, K.-H. Liao, D. Woll, J. Luu, C. Zhang, J. J. Morehead, J. Segall, J. Gregg, K. Tai, B. Kharlamov, H. Yu, and L. Myers, "Fused fiber pump and signal combiners for a 4-kW ytterbium fiber laser," in *Fiber Lasers VIII: Technology, Systems, and Applications*, 2011), 791431.

120. T. Ehrenreich, R. Leveille, I. Majid, K. Tankala, G. Rines, and P. Moulton, "1-kW, all-glass Tm: fiber laser," in *Fiber Lasers III: Technology, Systems, and Applications*, 2010), 758016.

121. N. Simakov, A. Hemming, S. Bennetts, and J. Haub, "Efficient, polarised, gain-switched operation of a Tm-doped fibre laser," Opt. Express **19**, 14949-14954 (2011).

122. A. M. Heidt, Z. Li, J. Sahu, P. C. Shardlow, M. Becker, M. Rothhardt, M. Ibsen, R. Phelan, B. Kelly, S. U. Alam, and D. J. Richardson, "100 kW peak power picosecond thulium-doped fiber amplifier system seeded by a gain-switched diode laser at 2 μm," Opt. Lett. **38**, 1615-1617 (2013).

123. C. W. Rudy, K. E. Urbanek, M. J. F. Digonnet, and R. L. Byer, "Amplified 2 μm Thulium-Doped All-Fiber Mode-Locked Figure-Eight Laser," Lightwave Technology, Journal of **31**, 1809-1812 (2013).

124. F. Qiang, K. Khanh, and N. Peyghambarian, "An All-Fiber 2-μm Wavelength-Tunable Mode-Locked Laser," Photonics Technology Letters, IEEE **22**, 1656-1658 (2010).

125. Q. Wang, T. Chen, B. Zhang, A. P. Heberle, and K. P. Chen, "All-fiber passively mode-locked thulium-doped fiber ring oscillator operated at solitary and noiselike modes," Opt. Lett. **36**, 3750-3752 (2011).

126. M. A. Solodyankin, E. D. Obraztsova, A. S. Lobach, A. I. Chernov, A. V. Tausenev, V. I. Konov, and E. M. Dianov, "Mode-locked 1.93 μm thulium fiber laser with a carbon nanotube absorber," Opt. Lett. **33**, 1336-1338 (2008).

127. J.-C. Diels and W. Rudolph, *Ultrashort laser pulse phenomena* (Academic press, 2006).

128. S. M. J. Kelly, "Characteristic sideband instability of periodically amplified average soliton," Electronics Letters **28**, 806-807 (1992).

129. R. H. Stolen, J. Botineau, and A. Ashkin, "Intensity discrimination of optical pulses with birefringent fibers," Opt. Lett. **7**, 512-514 (1982).

130. M. D. Nielsen, M. H. Sørensen, A. Liem, M. Kozak, and P. M. W. Skovgaard, "High-power PCF-based pump combiners," in *Fiber Lasers IV: Technology, Systems, and Applications*, 2007), 64532C.

131. D. Noordegraa, M. D. Nielsen, P. M. W. Skovgaard, S. Agger, K. P. Hansen, J. Broeng, C. Jakobsen, H. R. Simonsen, and J. Laegsgaard, "Pump combiner for air-clad fiber with PM single-mode signal feed-through," in *CLEO, Conference on Lasers and Electro-Optics*, 2009), CThGG.

132. D. Noordegraaf, M. D. Maack, P. M. W. Skovgaard, S. Agger, T. T. Alkeskjold, and J. Lægsgaard, "7+1 to 1 pump/signal combiner for air-clad fiber with 15 μm MFD PM single-mode signal feed-through," in *Fiber Lasers VII: Technology, Systems, and Applications*, 2010), 75801A.

133. B. G. Ward, J. D. L. Sipes, and J. D. Tafoya, "A monolithic pump signal multiplexer for air-clad photonic crystal fiber amplifiers," in *Fiber Lasers VII: Technology, Systems, and Applications*, 2010), 75801C.

134. J. D. L. Sipes, J. D. Tafoya, D. S. Schulz, B. G. Ward, and C. G. Carlson, "Advanced components for multi-kW fiber lasers," in *Fiber Lasers IX: Technology, Systems, and Applications*, 2012), 82370P.

135. D. L. Sipes, J. D. Tafoya, D. S. Schulz, B. G. Ward, and C. G. Carlson, "A 967 W single mode all-fiber PM Yb PCF fiber amplifier," in *Fiber Lasers VIII: Technology, Systems, and Applications*, 2011), 7914.

136. A. E. Siegman, "Defining, measuring, and optimizing laser beam quality," in *Laser Resonators and Coherent Optics: Modeling, Technology, and Applications*, 1993), 2-12.

137. S. Guillemet, Y. Hernandez, D. Mortag, F. Haxsen, A. Wienke, D. Wandt, L. Leick, and W. Richter, "High energy and low repetition rate picosecond thulium-doped all-fibre laser with photonic-crystal fibre amplifier," in *Advanced Solid-State Lasers Congress*, OSA Technical Digest (online) (Optical Society of America, 2013), ATu1A.5.

138. P. Kadwani, "Pulsed Tm-fiber Laser for Mid-IR Generation," (PhD Dissertation, CREOL, University of Central Florida, 2013).